Analysis of wind characteristics during Bora events in the southern region of Croatia

Topić, Roko

University of Split
Faculty of Science

Analysis of wind characteristics during Bora events in the southern region of Croatia

Master thesis

Roko Topić

April 2024, Split

Temeljna dokumentacijska kartica

Sveučilište u Splitu
Prirodoslovno – matematički fakultet
Odjel za fiziku
Ruđera Boškovića 33, 21000 Split, Hrvatska

Diplomski rad

Analiza karakteristika vjetra za vrijeme epizoda Bure na području južne Hrvatske

Roko Topić

Sveučilišni diplomski studij Fizika; smjer: Fizika okoliša

Sažetak:

Bura je sjeveroistočni vjetar s olujnim udarima koji puše duž jadranske obale. Prisutna je tijekom cijele godine, s tim da su češći i intenzivniji udari bure zimi. Područja sklona buri pogodna su za iskorištavanje energije vjetra. Bura se može manifestirati kao opasan vjetar koji utječe na građevine, prijevoz i ljude. Obično se javlja tijekom nekoliko karakterističnih sinoptičkih situacija nad Europom. Anticiklonalna i ciklonalna bura su najčešći oblici bure koji se pojavljuju duž jadranske obale. U južnom dijelu Hrvatske brdovit teren i nedostatak mjerenja predstavljaju izazov za razumijevanje dinamičkog nastanka bure. Za lokaciju Pometeno Brdo dobivena su mjerenja brzine i smjera vjetra. Podaci su dobiveni za prvo razdoblje od 2010. do 2011. godine, na 10 i 40 m visine iznad tla, te drugo razdoblje od 2018. godine, na 60 i 80 m visine iznad tla. Ovi podaci su filtrirani kako bi se ustanovile epizode bure koje traju duže od 10 sati. Nadalje, brzina i smjer vjetra preuzeti od Copernicus regional reanalysis for Europe (CERRA) su uspoređeni s opažanjima kako bi se procijenila točnost reanalize tijekom dostupnih epizoda bure. Također, odabrano je šest slučajeva bure za daljnju analizu i simulaciju putem Weather prediction and forecast (WRF) modela kako bi se odredili učinci poboljšanja prostorne razlučivosti na prikaz bure. Odabir svakog slučaja napravljen je s obzirom na tri čimbenika: sinoptička uvjeti nad južnom Hrvatskom, prosječna brzina bure i dostupnost podataka na različitim visinama iznad tla . Jenkinson-Collisonova automatizirana Lamb Weather Typing Classification shema koristi se za određivanje sinoptičkih vremenskih obrazaca nad južnom Hrvatskom tijekom svih dostupnih epizoda bure. Rezultati pokazuju zadovoljavajuću reprodukciju općeg ponašanja vjetra s CERRA-om za sve visine tijekom umjereno jakih epizoda bure. Brzina vjetra tijekom epizoda intenzivne bure reproducirana je s lošijom točnošću. WRF povećanje prostorne razlučivosti poboljšava reprodukciju brzine vjetra na svim visinama.

Ključne riječi: bura, brzina vjetra, sinoptički uvjeti, CERRA, WRF

Rad sadrži: 41 stranicu, 26 slika, 3 tablice, 15 literaturnih navoda. Izvornik je na engleskom jeziku.

Mentor: izv. prof. dr. sc. Žarko Kovač

Ocjenjivači: izv. prof. dr. sc. Žarko Kovač,
izv. prof. dr. sc. Jadranka Šepić,
doc. dr. sc. Ivana Weber

Rad prihvaćen: 12. Travanj, 2024.

Rad je pohranjen u Knjižnici Prirodoslovno – matematičkog fakulteta, Sveučilišta u Splitu.

Basic documentation card

University of Split
Faculty of Science
Department of Physics
Ruđera Boškovića 33, 21000 Split, Croatia

Master thesis

Analysis of wind characteristics during Bora events in the southern region of Croatia

Roko Topić

University graduate study Physics, specialization in Environmental Physics

Abstract:

Bora is a northeasterly, gusty wind which blows along the Adriatic coast. It is present during the whole year, with more frequent and more intense bora episodes appearing during wintertime. Bora-prone regions suitable for wind energy harvesting. Bora can be manifested as a hazardous wind affecting structures, transportation and people. It commonly occurs under a few characteristic synoptic settings over Europe. Anticyclonic and cyclonic bora are main types observed along the Adriatic coast. In the southern part of Croatia, complex terrain and scarcity of measurements make understanding of Bora dynamical generation challenging. Wind speed and direction measurements were obtained for the location of Pometeno Brdo. Data was obtained for the first period from 2010 to 2011, at 10 and 40 m heights above ground, and a second period from 2018, at 60 and 80 m heights above ground. This data was filtered to distinguish bora wind episodes, lasting longer than 10 hours. Furthermore, Copernicus regional reanalysis for Europe (CERRA) produced wind speed is compared to the observations to evaluate the accuracy of the reanalysis during available bora episodes. Additionally, six Bora case studies are selected for further analysis and Weather prediction and forecast (WRF) model simulation to determine the effects of spatial downscaling on bora wind representation. The study case period selection is made regarding three factors: synoptic setting over southern Croatia, average bora wind speed and data availability at different heights above ground. Jenkinson-Collison automated Lamb Weather Typing Classification scheme is used to determine the synoptic weather patterns over southern Croatia during all available bora episodes. Results show satisfactory reproduction of general wind behavior with CERRA for all heights during moderately strong bora episodes. Wind speed during intense bora episodes is reproduced with poor accuracy. WRF downscaling improves wind speed reproduction on all heights.

Keywords: bora, wind speed, synoptic setting, CERRA, WRF

Thesis consists of: 41 pages, 26 figures, 3 tables, 15 references. Original language: English.

Supervisor: Assoc. Prof. Dr. Žarko Kovač

Reviewers: Assoc. Prof. Dr. Žarko Kovač,
Assoc. Prof. Dr. Jadranka Šepić,
Assist. Prof. Ivana Weber

Thesis accepted: April 12, 2024

Thesis is deposited in the library of the Faculty of Science, University of Split.

I would like to thank my professor and mentor Žarko Kovač for assistance and constructive communication during my master study. I would also like to thank professor Jadranka Šepić for motivation and opportunities that she highlights for us, students. I am very thankful to Petra Lepri and professor Branko Grisogono who provided valuable data on behalf of Geophysics department of Faculty of Science, Zagreb. Also, I would like to thank prof. Gunilla Svensson and Pall Thorarinsson from KTH, Sweden, as they provided much needed support and friendly advice during my research. Additional thanks to Mirko Kovačević who provided data on behalf of Končar d.o.o.
Lastly, I would like to thank my family, friends and colleagues.

Contents

1 Introduction

Dalmatia is a wind-prone region in the southern part of Croatia (Figure 1). Similarly to the north Adriatic coast of Croatia, in Dalmatia as well, bora is one of the strongest winds affecting buildings, roads, air and sea transportation. Bora is often categorized as a gusty, downslope wind of NE direction blowing across the steep Dinaric mountain chain. Although dynamical generational mechanisms for bora flow are more complex and less researched for the south than for the north Adriatic [1], its general directional and intensity characteristics are of similar nature to its north Adriatic counterpart.

It has been shown that bora wind appears more severe in wintertime with episodes lasting continuously for a few days, while in summertime, its persistence is shorter and intensity milder. Bora wind is linked with mesoscale distributions of mean sea level pressure (MSLP) and geopotential height at 500 hPa over Europe. A few categories of bora are presented with respect to this, most notably anticyclonic (clear), cyclonic (dark) and frontal bora [2].

Due to delicate observational equipment and difficult terrain not many field measurements of bora have been made in Dalmatia. One of exceptions is a field campaign done in 2010 to 2011, results of which are given in with Lepri et al. [3]. Results of this measurement campaign and further data analysis at the location of Pometeno Brdo (Figure 2) have given valuable insight into the near surface structure of bora wind. Additionally, wind farms, such as one the built also on the location of Pometeno Brdo by Končar d.o.o., collect hourly-averaged wind speed and direction data at wind turbine hub height. This information is commonly used to address wind resources for the needs of energy production but also presents a valuable set of information for wind analysis.

Development in computational capabilities allows numerical simulations of micro- and mesoscale atmospheric behavior to become more feasible with methods like LES, providing high accuracy description of turbulent motions in bora regime, [4]. As both the measuring campaigns and LES models present a costly option for prolonged surveillance of wind behavior at a location of interest, climatological reanalysis such as CERRA can be a useful alternative (shown in [5] and [6]). In addition to CERRA, Weather prediction and forecast (WRF) numerical model is able to produce a high-resolution weather forecast and hindcast with customizable input and output precision. This makes WRF a practical tool for simulation of wind parameters during periods of interest, as seen in [7].

Knowledge on bora persistence during the year and hourly wind speed variations of bora wind is crucial for infrastructure planning and wind energy industry. In this study, measurements of wind speed and direction obtained for two distinct periods at three nearby locations, on four near-surface vertical heights, have been used to distinguish bora episodes. This allowed for a systematic analysis of wind speed and categorization of synoptic settings over southern Croatia for all available bora episodes. Mesoscale models have already been used for representation of bora episodes on the northern Adriatic coast with satisfactory results [8]. My analysis shows that CERRA and WRF products can be used for wind resource assessment in the region of Dalmatia. Mean wind speed of all available bora episodes was compared to CERRA products. Additionally, benefits of WRF spatial downscaling on accuracy of wind speed representation have been tested for six case studies.

Figure 1
Region of Dalmatia.

2 Theoretical background

Fundamental statements that describe ABL physics are the following governing equations. These equations are a starting point for every numerical weather model and are presented below:
Equation of state:

$$p = \rho_{air} R T_v \tag{2.1}$$

Conservation of mass:

$$\frac{\delta \rho}{\delta t} + \rho \frac{\delta U_j}{\delta x_j} = 0 \tag{2.2}$$

Conservation of momentum:

$$\frac{\delta U_i}{\delta t} + U_j \frac{\delta U_i}{\delta x_j} = -\delta_{i3} g - 2\epsilon_{ijk} \Omega_j U_k - \frac{1}{\rho} \frac{\delta p}{\delta x_i} + \frac{1}{\rho} \frac{\delta \tau_{ij}}{\delta x_j} \tag{2.3}$$

Conservation of moisture:

$$\frac{\delta q_T}{\delta t} + U_j \frac{\delta q_T}{\delta x_j} = v_q \frac{\delta^2 q}{\delta x_j^2} + \frac{S_{qT}}{\rho_{air}} \tag{2.4}$$

Conservation of heat:

$$\frac{\delta \Theta}{\delta t} + U_j \frac{\delta \Theta}{\delta x_j} = v_\Theta \frac{\delta^2 \Theta}{\delta x_j^2} - \frac{1}{\rho C_p} \frac{\delta Q_j^*}{\delta x_j} - \frac{L_p E}{\rho C_p} \tag{2.5}$$

Pressure is denoted as p. $\rho_a ir$ is the density of moist air. T_v is the virtual absolute temperature. R is the gas constant for dry air. U_i is a component of velocity vector along x axis (same analogy for j - y axis and k - z axis). Ω_j is an angular velocity vector of the earth's rotation. g is a gravitational constant and τ_{ij} is deviatoric stress tensor. q_T is the total specific humidity of air (all phases) and q is the specific humidity of air. V_q is the molecular diffusivity for water vapor in the air. S_{qT} is a net moisture source term (sources - sinks) for the remaining processes not already included in the equation. v_Θ is the thermal diffusivity, and L_p is the latent heat associated with the phase change information - E. Q_j^* is the component of net radiation in the j^{th} direction. The specific heat for moist air at constant pressure is denoted as C_p.
Further simplification and scaling of the governing equations is applied with use of convectional approximations for the ABL, such as Boussinesq rule for density variations and Reynolds decomposition of quantities to its mean and perturbation counterparts. This leads to expressions for turbulent fluxes and convenient parameters, such as turbulent kinetic energy (TKE), 2.6. The equations are eventually reduced by this process to a system with number of unknown variables being larger than the number of equations. Here lies the closure problem of turbulent motion and is dealt with Mellor-Yamada-Janjić (MYJ) closure scheme that is implemented in the WRF numerical model used in this study.

Derived TKE budget equation:

$$\frac{\delta\overline{e}}{\delta t} + \overline{U_j}\frac{\delta\overline{e}}{\delta x_j} = +\delta_{i3}\frac{g}{\overline{\Theta_v}}(\overline{u_i'\theta_v'}) - \overline{u_i'u_j'}\frac{\delta\overline{U_i}}{\delta x_j} - \frac{\delta(\overline{u_j'e})}{\delta x_j} - \frac{1}{\overline{\rho}}\frac{\delta(\overline{u_i'p'})}{\delta x_i} - \epsilon \tag{2.6}$$

Definition of TKE is $\overline{e} = \overline{(u_i'^2)}$. First term in eq 2.6 presents local storage of TKE, second term presents advection of TKE by mean wind, third term displays buoyancy consumption/production, fourth term shows mechanical production/consumption, fifth term presents turbulent transport, sixth term describes pressure correlation, and seventh term is dissipation of TKE.

The Mellor-Yamada Level 2.5 turbulence closure model (MY 2.5) central equations:

$$\frac{\delta}{\delta t}\left(\frac{q^2}{2}\right) - \frac{\delta}{\delta z}\left[lqS_q\frac{\delta}{\delta z}\left(\frac{q^2}{2}\right)\right] = P_s + P_b - \epsilon \tag{2.7}$$

$$P_s = -\overline{w'u'}\frac{\delta\overline{U}}{\delta z} - \overline{w'v'}\frac{\delta\overline{V}}{\delta z} \tag{2.8}$$

$$P_b = \beta g\overline{w'\theta_v'} \tag{2.9}$$

$$\epsilon = \frac{q^3}{lB_1} \tag{2.10}$$

$$\overline{wu} = -K_M\frac{\delta U}{\delta z}; \quad \overline{wv} = -K_M\frac{\delta V}{\delta z}; \quad \overline{w\theta'} = -K_H\frac{\delta\Theta}{\delta z} \tag{2.11}$$

$$K_M = lqS_M; \quad K_H = lqS_H \tag{2.12}$$

$$S_M(6A_1A_2G_M) + S_H(1 - 3A_2B_2G_H - 12A_1A_2G_H) = A_2 \tag{2.13}$$

$$S_M(1 + 6A_12G_M - 9A_1A_2G_H) - S_H(12A_12G_H + 9A_1A_2G_H) = A_1(1 - 3C_1) \tag{2.14}$$

$$G_M = \left(\frac{l^2}{q^2}\right)\left[\left(\frac{\delta U}{\delta z}\right)^2 + \left(\frac{\delta V}{\delta z}\right)^2\right]; \quad G_H = -\left(\frac{l^2}{q^2}\right)\beta g\frac{\Theta_V}{\delta z} \tag{2.15}$$

TKE in MY 2.5 is in form of $\frac{1}{2}q^2$ for clarity. $S_q = 0.2, \beta = 1/273$ and following constants: A_1, A_2, B_1, B_2 are determined experimentally. l is the master length scale, K_H and K_M are the vertical turbulent exchange coefficients for heat and momentum respectively. P_s and P_b are the terms describing the production of turbulent kinetic energy due to shear and buoyancy. The dissipation is denoted by ϵ. Presented set of equations, when master length scale is determined, lead to a solution of closure problem and with additional contribution from Janjić [9], provide a core of MYJ closure scheme.

For wind speed vertical interpolation power low has been used in this study (2.16). Description of wind profile using power law for the location of Pometeno Brdo was inspecte by Lepri et al. [3].

$$\frac{u}{u_r} = \left(\frac{z}{z_r}\right)^{\alpha} \tag{2.16}$$

Wind speed at height z is denoted with u, and u_r is the known wind speed at a reference height z_r. The exponent α is calculated from wind speed values at known heights.

3 Data and Methods

Wind speed and wind direction data at 10 and 40 meters above ground were measured at Pometeno Brdo during a field-measuring expedition (Lepri et al. [3]). The meteorological mast with measuring stations was located at 43° 36’ 28.9” N, 16° 28’ 37.4” E (Figure 2) and operational in the period from April 2010 to June 2011. Starting and ending dates of 119 bora episodes, mean wind speed and duration of each episode are given in the Table 1 in work of Lepri et al. [3]. Additionally, wind speed and direction measurements were also done by Končar d.o.o. at two locations at Pometeno Brdo from January to December 2018. This dataset contains data from anemometers placed on the wind turbines, at hub height, of two different-sized aggregates, one at the location 43° 36’ 31.2" N, 16° 28’ 30.7" E with hub height of 60 m and the other at location 43° 36’ 36.3" N, 16° 28’ 39.5" E with hub height of 80 m (Figure 2). All unrealistic values were removed from data by application of visual quality control. Bora episodes were extracted using filtering rules suggested by Lepri et al. [3], resulting with 43 bora episodes longer than 10 hours (Table 1) in January-December 2018.

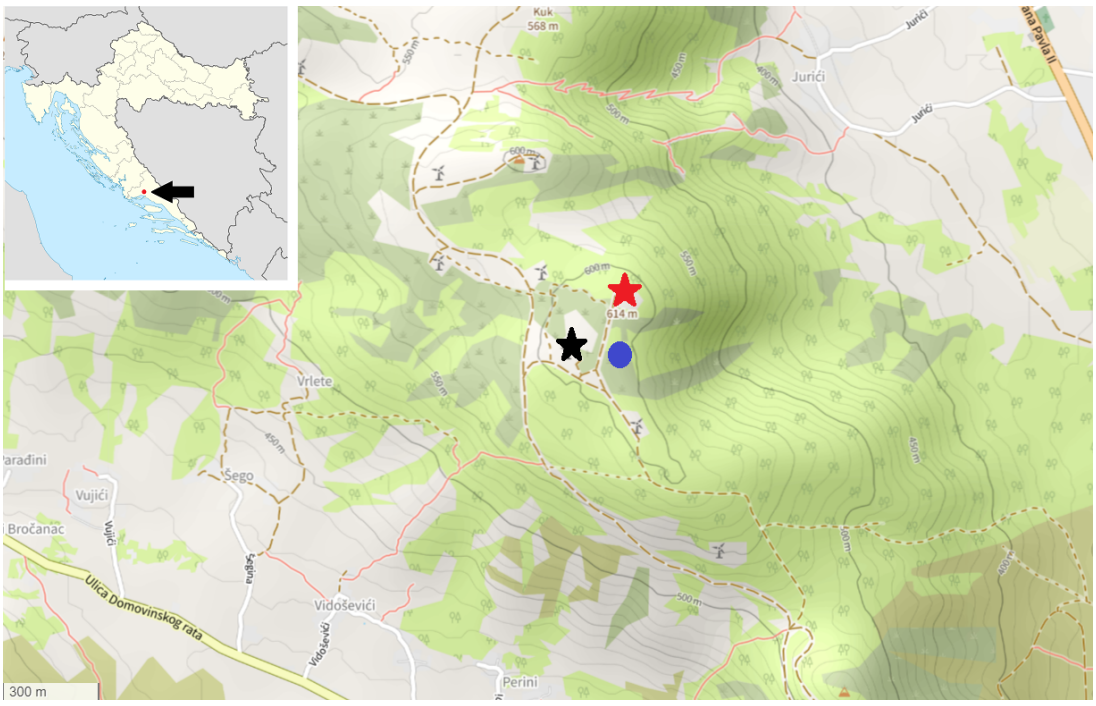

Figure 2
Terrain configuration at Pometeno Brdo. Red star marks the location of the wind turbine with hub height of 80 m, black star marks the location of the wind turbine with hub height of 60 m and blue circle marks the location where meteorological mast was placed (2010-2011).

Bora episode no.	Start time	End time	Duration (h)	V_{60mean} (m/s)	V_{80mean} (m/s)	V_{60max} (m/s)	V_{80max} (m/s)
1	20.1. 00:00	20.1. 11:00	11	7.1	5.7	9.9	8.1
2	21.1. 17:00	22.1. 12:00	19	15.9	13.2	23.6	21.3
3	23.1. 08:00	24.1. 09:00	25	9.4	7.8	14.3	12
4	09.2. 22:00	11.2. 18:00	44	11.3	9.3	20.3	16.9
5	13.2. 13:00	16.2. 02:00	61	7.7	6.1	16.9	14.7
6	18.2. 09:00	20.2. 01:00	40	9.6	7.9	12.1	10.5
7	20.2. 18:00	22.2. 01:00	31	9.8	8.3	13.1	11.4
8	23.2. 21:00	27.2. 10:00	85	11.4	9	17.9	14.9
9	27.2. 20:00	01.3. 01:00	29	6.8	5.1	10.6	8
10	20.3. 20:00	24.3. 11:00	87	15.6	16.5	24.6	24.3
11	25.3. 19:00	26.3. 09:00	14	6.2	5.8	10.1	10.3
12	26.3. 23:00	27.3. 10:00	11	5.4	5.1	7.2	6.9
13	06.4. 04:00	07.4. 09:00	29	9.2	10.3	16.6	17
14	17.4. 17:00	19.4. 10:00	41	12.4	10.4	19.4	16.6
15	19.4. 19:00	21.4. 07:00	36	9.4	10	15.1	17.1
16	26.4. 22:00	27.4. 09:00	11	6.8	5.6	11.3	9.8
17	05.5. 22:00	06.5. 14:00	16	9.3	9.2	15.1	16.1
18	06.5. 16:00	08.5. 10:00	42	8	8	13.3	14.3
19	19.5. 00:00	20.5. 10:00	30	5.2	5.8	7.9	9.2
20	20.5. 19:00	21.5. 07:00	12	6.7	7.2	9.7	11.8
21	14.6. 02:00	17.6. 01:00	71	7.6	10.1	12.2	14.8
22	17.6. 19:00	20.6. 09:00	62	9	11.1	15.9	18.3
23	27.6. 11:00	27.6. 23:00	12	9.7	10.4	13.9	15
24	08.7. 08:00	09.7. 23:00	31	11.1	9.7	15.6	14.7
25	23.7. 13:00	25.7. 13:00	48	9.2	9.6	15	15.9
26	25.7. 20:00	26.7. 11:00	15	7.3	8.3	9.3	9.7
27	29.7. 19:00	30.7. 15:00	20	6.8	6.8	9.4	9.6
28	30.7. 19:00	31.7. 12:00	17	7.8	9.4	11.1	14.1
29	02.8. 16:00	03.8. 14:00	22	6.2	6.8	9.1	10.3
30	03.8. 19:00	04.8. 11:00	16	6.6	5.3	8.4	7
31	15.8. 04:00	16.8. 15:00	35	7.6	10.2	10.8	14.8
32	19.8. 19:00	20.8. 12:00	17	7.4	7.7	11.1	12.4
33	26.8. 22:00	29.8. 08:00	58	7	7.1	13.4	15.5
34	24.9. 10:00	26.9. 07:00	45	19.1	19	25.4	25.4
35	26.9. 10:00	28.9. 07:00	45	5.9	6.4	13.2	11.1

Bora episode no.	Start time	End time	Duration (h)	V_{60mean} (m/s)	V_{80mean} (m/s)	V_{60max} (m/s)	V_{80max} (m/s)
36	28.9. 22:00	30.9. 14:00	40	11.6	12.3	21	20.5
37	19.10. 20:00	23.10. 17:00	93	11.1	10.1	20.8	20
38	24.10. 21:00	25.10. 08:00	11	11.1	9.6	16.1	15.7
39	14.11. 01:00	19.11. 08:00	127	5.7	4.8	18.2	16.6
40	27.11. 00:00	30.11. 07:00	79	11.7	9.6	21.5	18.6
41	04.12. 12:00	05.12. 16:00	26	11.4	9.5	17	14.4
42	08.12. 14:00	09.12. 02:00	12	10.8	9.1	15.4	13.6
43	10.12. 05:00	10.12. 22:00	17	7.8	6.3	13.6	11

Table 1

Extracted bora episodes at Pometeno Brdo in 2018. Wind speed at 60 and 80 m heights is also given.

3.1 Reanalysis and WRF

CERRA is a climate reanalysis made available by Copernicus climate change service project monitored by the European Centre for Medium-Range Weather Forecasts (ECMWF). The CERRA reanalysis dataset was downloaded in temporal resolution of 3 hours at a grid resolution of 5.5 km for both 2010-2011 and 2018. For this study, wind speed and direction values at vertical levels of 10, 15, 30, 50 and 75 m were acquired from CERRA. For better comparison and visualization of data, wind speed was interpolated to the height of each available measuring station using the power law (Eq. 2.16). Wind direction was directly compared to the nearest measuring height. ERA5 is also an ECMWF reanalysis dataset. It was used for a boundary and initial conditions for WRF model. Resolution of ERA5 is 31 km. It was chosen over CERRA dataset because of the faster are more practical implementation into WRF.

WRF model was used to simulate selected parameters at a 1km resolution, with temporal output of 15 min. One parent and two nested domains were used in WRF (Figure 3). Model physics and dynamics were the same as used by Kuzmić et al. [10] with a significant increase in density of the near-surface vertical levels, closely resembling vertical resolution provided by CERRA. Terrain data, used in WRF domains, is prepared identical as in work of Solbakken et al. [7]. WRF simulation was run for total of six case studies.

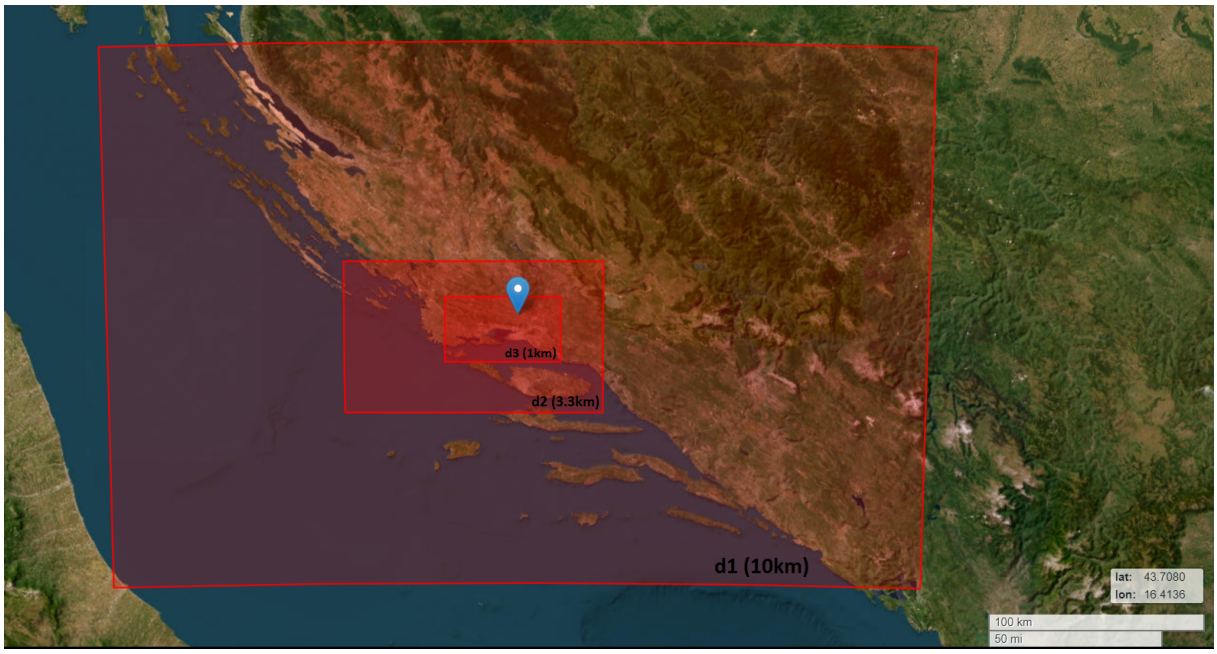

Figure 3
Domains of WRF simulation labeled as d1,d2 and d3 with their respective grid resolutions.

3.2 Synoptical and seasonal categorization

First distinction made between bora episodes was to separate them into summertime, May to September, and wintertime, October to April, season as bora is shown to notably differ in its intensity depending on the time of year, [11].
Furthermore, bora episodes have been linked with two prominent synoptical settings over Europe, namely anticyclonic (clear) and cyclonic (dark). Anticyclonic bora is corelated to a mean sea level pressure (MSLP) high over central Europe that gradually descends along Dinaric mountains bringing anticyclonic weather to the Adriatic coast (5a). Also, a thorough in geopotential height at 500hPa is visible during Anticyclonic bora extending from northeastern Europe towards the south Balkans (5b). Cyclonic bora is formed after a pressure low positioned over central Mediterranean moves south-east along the Balkan peninsula (6a). Thorough in geopotential height for this case extends towards central Mediterranean (6b).
To determine which synoptical weather pattern was dominant over southern Croatia for the duration of each bora episode, The Jenkinson-Collison automated Lamb Weather Typing Classification scheme (JC-WT) was utilized, [12] . Weather type index, divided into anticyclonic (A), cyclonic (C) and 8 different main directions of geostrophic flow (N, E, W, S, NE, NW, SE, SW), was calculated for both measuring periods, every 6 hours using ERA5 data.

Each recorded bora episode is categorized into one of 10 mentioned categories by the frequency of circulation pattern assessed for every 6-hour time step during the bora episode. Events where no type was dominant for at least half of the bora episode were assigned an uncategorized (U) type. Location selected for the JC classification scheme central point is Pometeno Brdo with coordinates identical to that of the meteorological mast placement (4).

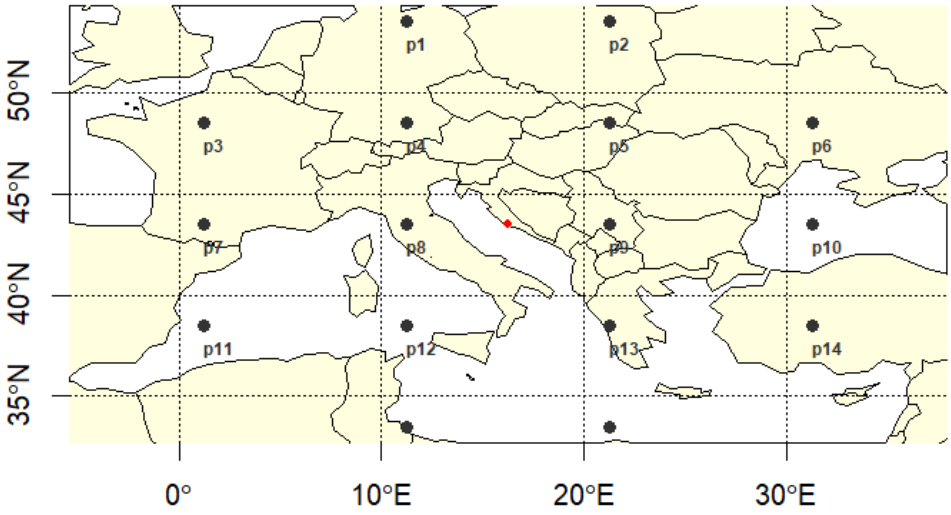

Figure 4
JC-WT scheme point selection - each point represents a location from which MSLP value was considered for calculation of weather indices.

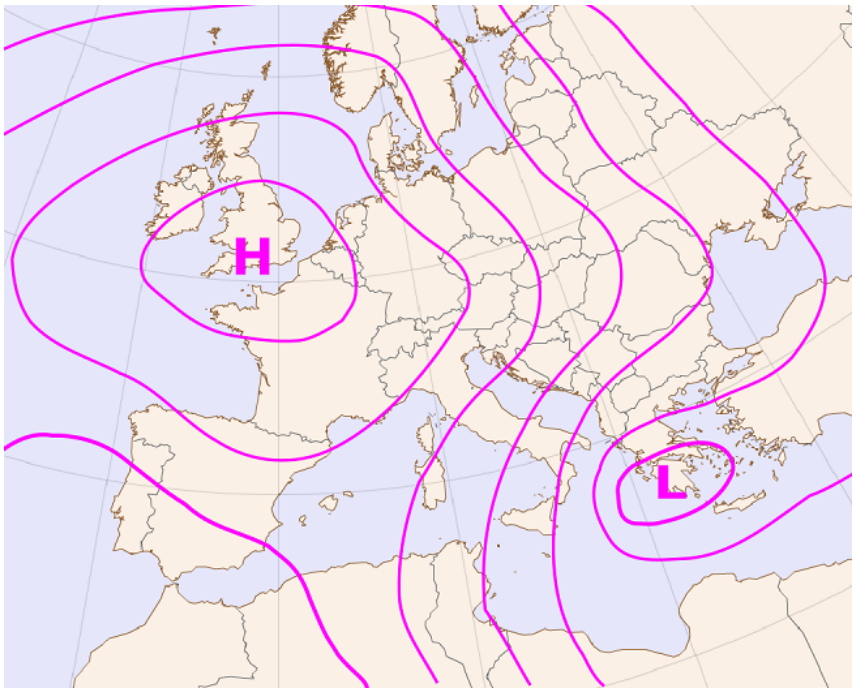

(a) *Mean sea level pressure map during anticyclonic bora. H - representing the center of heigh pressure. L - represening the center of low pressure.*

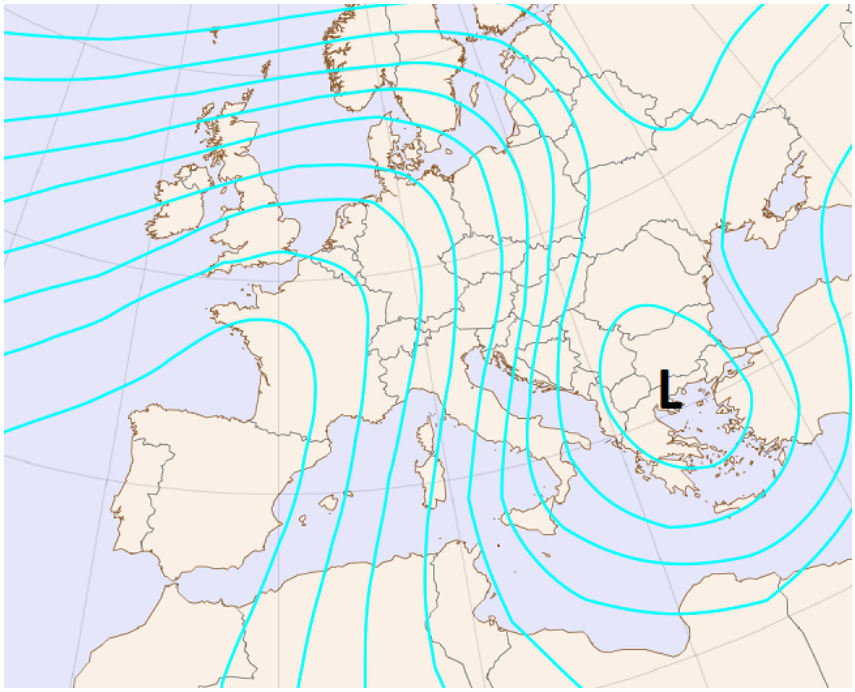

(b) *Geopotential height at 500 hPa during anticyclonic bora, L - representing the local minimum of geopotential height.*

Figure 5: *Typical MSLP and geopotential height distribution over Europe during anticyclonic bora.*

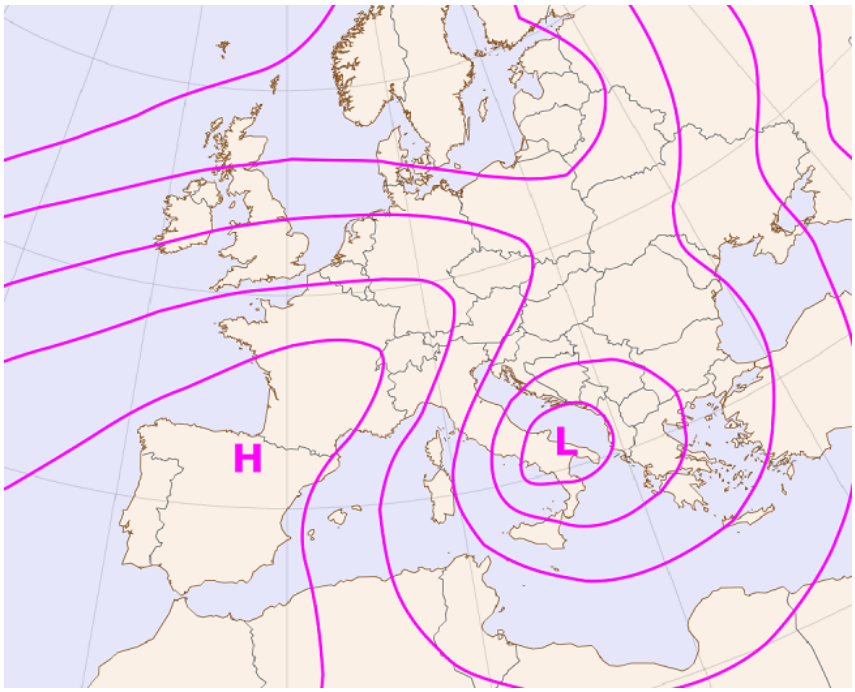

(a) *Mean sea level pressure map during cyclonic bora. H - representing the center of heigh pressure. L - represening the center of low pressure.*

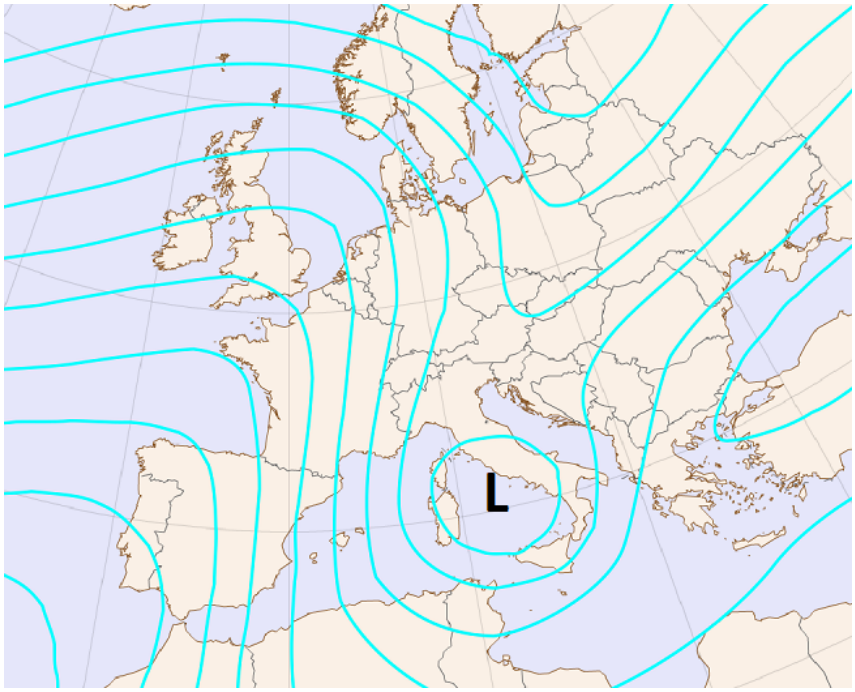

(b) *Geopotential height at 500 hPa during cyclonic bora, L - representing the local minimum of geopotential height.*

Figure 6: *Typical MSLP and geopotential height distribution over Europe during cyclonic bora.*

4 Results

4.1 Bora episode representation in CERRA

Mean wind speed calculated from CERRA dataset underestimates the measured averages for most bora episode on 10 and 40 m heights. At 10 m height, there is an average underestimation between observed values and CERRA of 2.7 ms^{-1} (Figure 7a). This is somewhat improved for 40 m height with 1.1 ms^{-1} total underestimation (Figure 7b). There are 68 Bora episodes recorded in wintertime and 51 in summertime (Table 1 [3]).

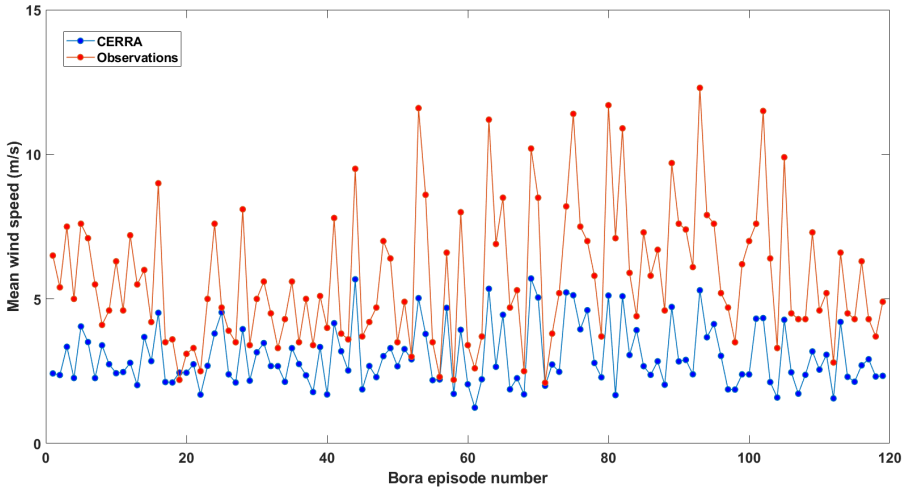

(a) *Mean wind speed values for bora episodes in years 2010-2011 at 10m height*

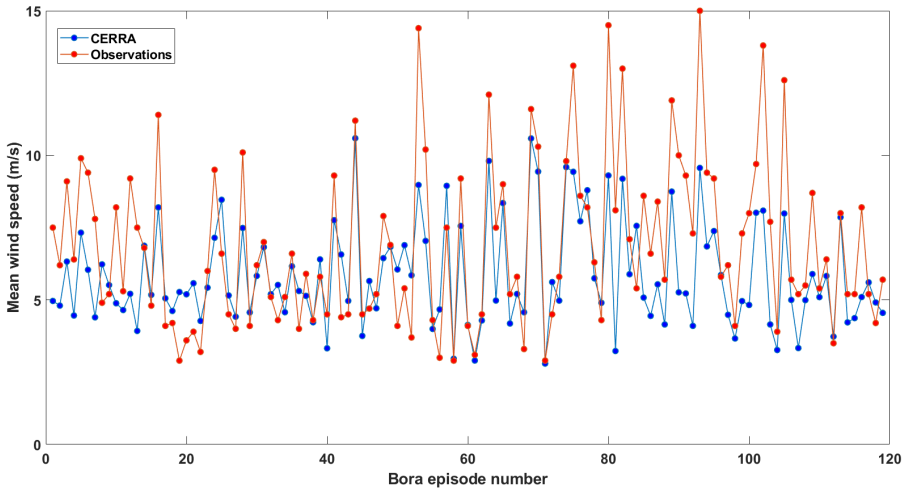

(b) *Mean wind speed values for bora episodes in year 2010-2011 at 40m height*

Figure 7: *Observed and CERRA wind speed averages for 119 bora episodes from Table 1 [3]*

Bora episodes with lowest wind speed averages are well represented by CERRA at 10 m height and frequently overestimated at 40 m height (Figure 8). At high wind speed episodes, CERRA underestimation reaches up to 7 ms^{-1} at 10 m height and 5 ms^{-1} at 40 m height.

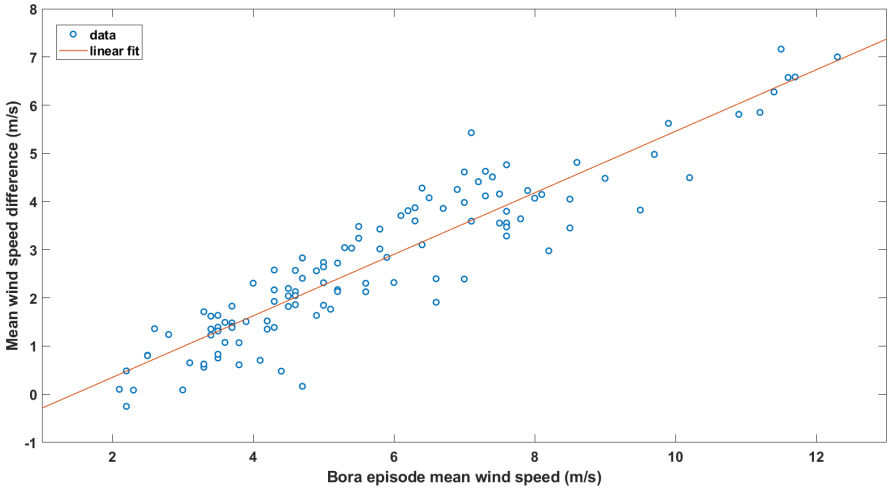

(a) *Difference between observed and CERRA mean wind speed values versus mean observed wind speed for year 2010/2011 at 10 m height, for bora episodes.*

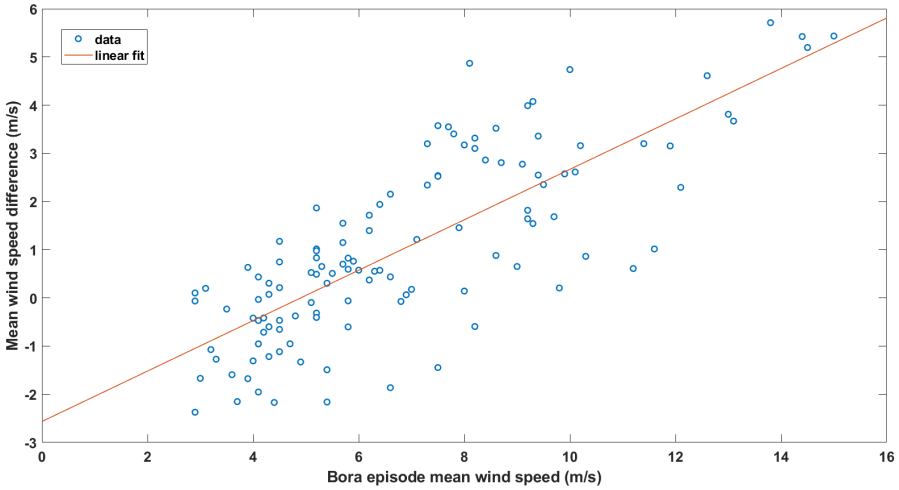

(b) *Difference between observed and CERRA mean wind speed values versus mean observed wind speed for year 2010/2011 at 40 m height, for bora episodes.*

Figure 8: *Difference between observed and CERRA wind speed averages compared to observed wind speed for the events presented in Figure 7. Linear fit is applied.*

Comparison of bora episodes in 2018 gives high discrepancies for both 60 m and 80 m heights between observational and CERRA data with average reanalysis underestimation of 3.1 and 2.2 $ms^{-}1$ respectively (Figures (9a) and (9b). There are 23 bora episodes recorded in wintertime and 20 in summertime (Table 1).

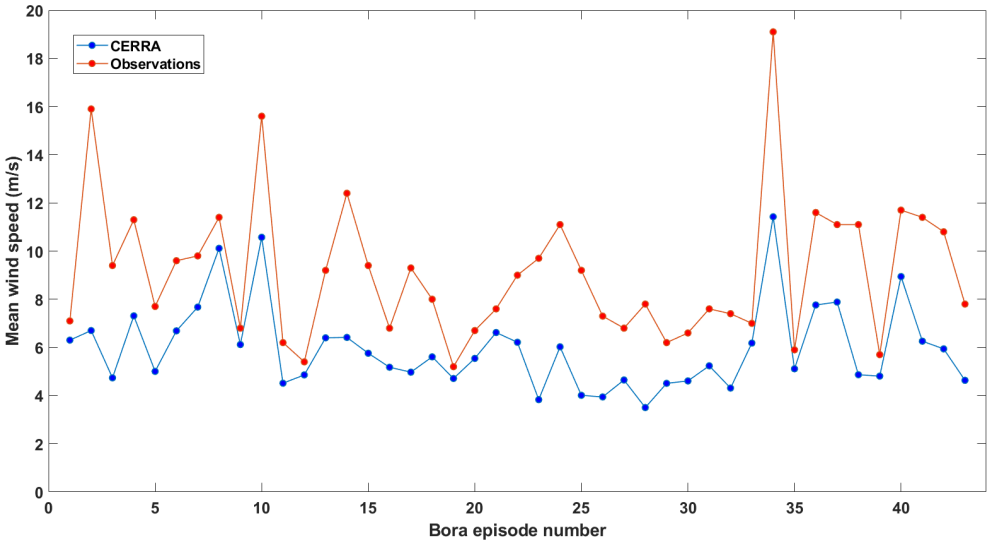

(a) *Mean wind speed values for bora episodes in year 2018 at 60m height*

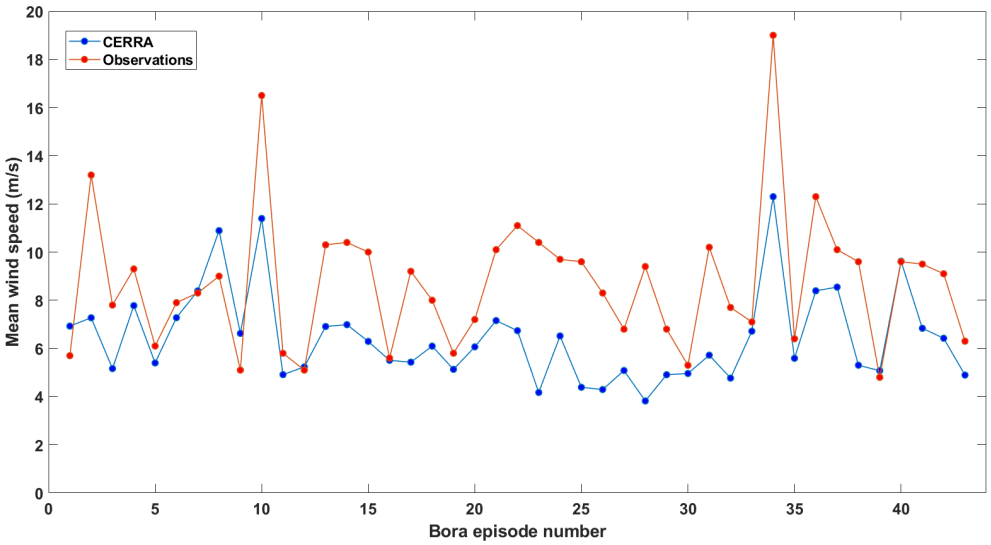

(b) *Mean wind speed values for bora episode in year 2018 at 80m height*

Figure 9: *Observed and CERRA wind speed averages for 43 bora episodes from Table 1 1. Linear fit is applied.*

At 60 m and 80 m height for bora episodes with low average wind speed are moderately underestimated by CERRA by up to 6 $ms^{-}1$ (Figure 10). At 80 m height there is an overestimation of low wind speed episodes by up to 2 $ms^{-}1$ (Figure 10b). With increase of average wind speed per episode, underestimation by CERRA rises at both heights.

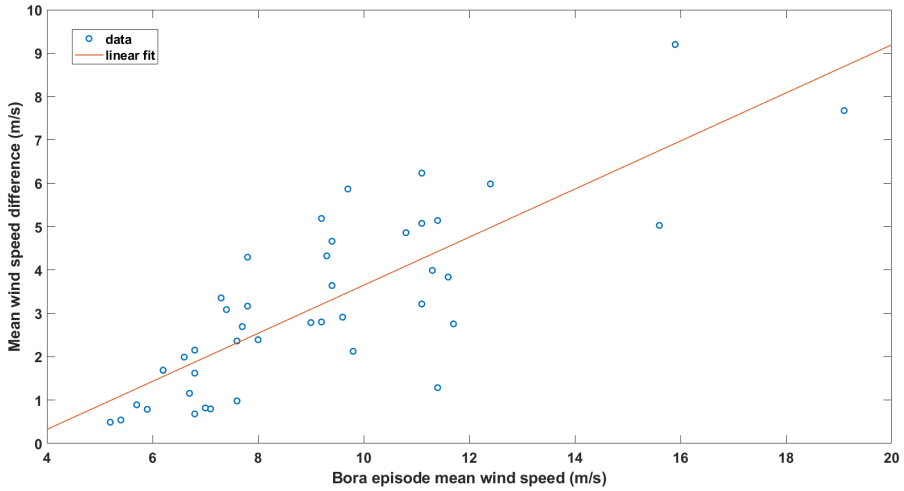

(a) *Difference between observed and CERRA mean wind speed values versus mean observed wind speed for year 2018 at 60 m height, for bora episodes.*

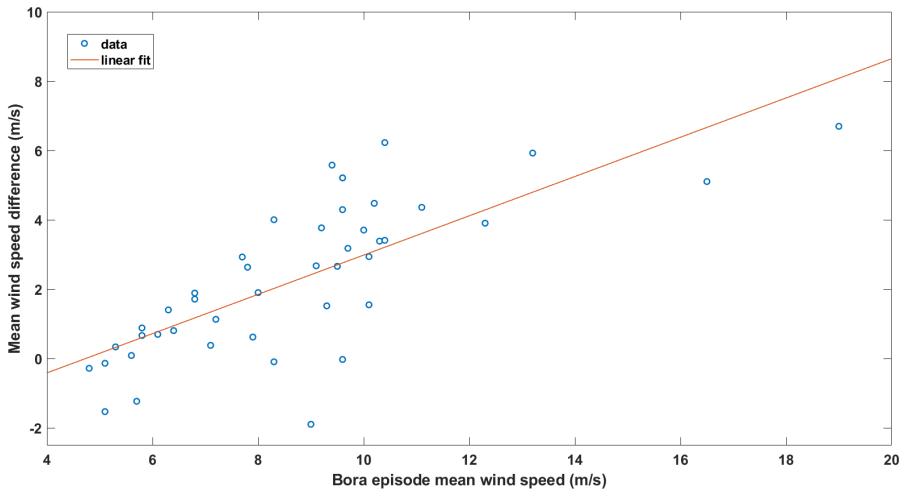

(b) *Difference between observed and CERRA mean wind speed values of Bora episodes versus mean observed wind speed for year 2018 at 80 m height, for bora episodes.*

Figure 10: *Difference between observed and CERRA wind speed averages compared to observed wind speed for the events presented in Figure 9. Linear fit is applied.*

In the period of 2010 to 2011, 20 summertime and 14 wintertime bora episodes from Table 1 referenced in Lepri et al., [3] are categorized using JC-WT scheme as A type event (Figure 11a). Average wind speed observational data is lowest for A type bora episodes (Table 2) when compared to all other types. Average wind speed of easterly (E) categorized bora episodes is the highest among all other types, in winter and summertime, respectively. Southeasterly (SE) type bora episodes are frequent in wintertime, contrary to northeasterly (NE) type bora episodes which persist mostly during summertime. C type is linked to 11 bora episodes, equally distributed in the summertime and wintertime, with average wind speed of 5 to 6 ms^{-1}. There is total of 26 uncategorized bora episodes in this period amounting to 21% of all bora episodes recorded by Lepri et al. [3]. CERRA reanalysis underestimates mean wind speed for each bora type at 10 m by up to 50% and shows considerable underestimation of mean wind speed for NE and E categories at 40 m level. Median duration of JC-WT classified bora episodes shows highest value of 27h for U type and 25h for E type category. All other categories with more than one bora episode have median duration of 13 to 16h.

		Observations				CERRA			
		2010/2011		2018		2010/2011		2018	
		10m	40m	60m	80m	10m	40m	60m	80m
A	W	4.5	5.4	8.5	8.2	2.7	5.2	5.2	5.7
	S	4.5	5.5	N/A	N/A	2.5	5.1	N/A	N/A
C	W	5.3	6.2	7.1	6.4	2.9	5.7	5.7	6.1
	S	4.8	5.9	N/A	N/A	2.5	5.1	N/A	N/A
E	W	8.4	9.7	12.4	11.5	4.5	8.4	8.5	9.1
	S	6.1	7.3	6.6	7.1	3.2	6.1	4.7	5.1
NE	S	5.9	7.5	8.5	7.1	2.8	5.2	4.7	5.1
SE	W	5.6	6.3	N/A	N/A	2.9	6	N/A	N/A

Table 2

Observed and CERRA reproduced mean wind speed for bora episodes in 2010/11 and 2018 categorized by JCWT scheme. S stands for summertime and W for wintertime. Data for categories with almost no bora episodes are not shown.

In 2018, most of the bora episodes measured at 60m and 80m levels are linked to E or NE directional type (Figure 11b). Mean wind speed of bora episodes categorized as E type in wintertime is highest among all categories and has been underestimated by approximately 2.9 $ms^{-}1$ at 60m and by 2.4 $ms^{-}1$ at 80m level with CERRA (Table 2).

Other categories also show a greater underestimation of observed mean wind speed by CERRA at 60m level than at 80m level. There is total of 6 uncategorized bora episodes during this period amounting to 14% of all bora episodes from presented in Table 1. Calculated median duration of bora episodes for E, U and A categories spans from 36 to 40 h while all other categories with more than one bora episodes have median duration of 14 to 20 h.

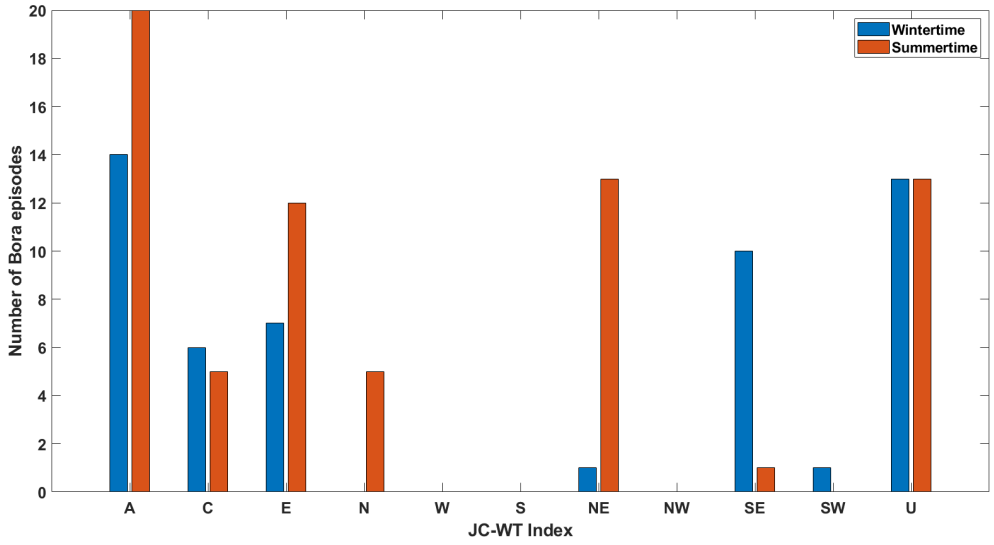

(a) *JC-WT index distribution for 119 bora episodes in 2010-2011.*

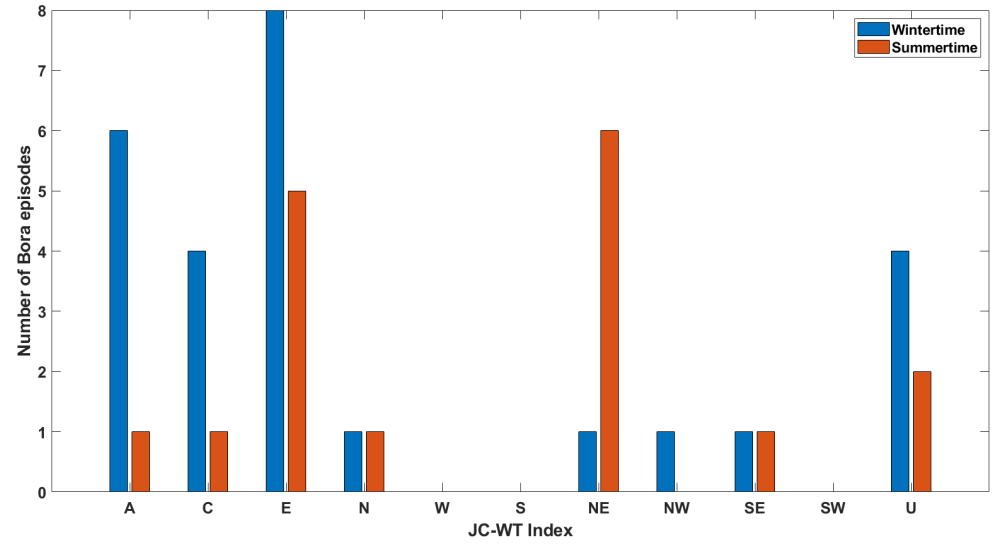

(b) *JC-WT index distribution for 43 bora episodes in 2018.*

Figure 11: *Distribution of JC-WT scheme produced indices for bora episodes during periods of interest.*

4.2 Case study analysis

Bora episodes labeled as A, C and U type by JC-WT scheme were selected for WRF simulation. This was done for 2010-2011 and 2018, respectively. Although E type bora episodes appear more often during both periods, A and C type episodes were chosen to represent anticyclonic and cyclonic bora. U type episode longer than three days was selected to analyze synoptic settings and wind speed variations over a longer period. Most of the low wind speed A type episodes are preceded by a strong bora episode of directional or U type (not shown) and are included in the analysis. The WRF model reproduces the observed mean speed value better than CERRA (Table 3).

		Case 1	Case 2	Case 3	Case 4	Case 5	Case 6
		Mean wind speed (m/s)					
10m	Observations	9.9	N/A	11.3	N/A	10.8	N/A
	WRF	7.7	N/A	8.6	N/A	7.3	N/A
	CERRA	4.5	N/A	5.5	N/A	5.6	N/A
40m	Observations	12.1	N/A	13.6	N/A	11.6	N/A
	WRF	8.8	N/A	9.8	N/A	8.4	N/A
	CERRA	7	N/A	8.4	N/A	8.7	N/A
60m	Observations	N/A	13.3	N/A	13.4	N/A	11.4
	WRF	N/A	10.3	N/A	10.9	N/A	10.3
	CERRA	N/A	9	N/A	9.2	N/A	9.3
80m	Observations	N/A	13	N/A	14	N/A	9.3
	WRF	N/A	11.2	N/A	11.8	N/A	11.3
	CERRA	N/A	9.7	N/A	9.9	N/A	9.9

Table 3

Mean wind speed for six selected bora case studies calculated from observations, CERRA and WRF.

1) U type bora episode No. 80 and A type bora episode No. 81 were selected as the first case study (Table 1, Lepri et al.).
2) E type bora episode No. 35 and A type bora episode No. 36 have been selected for the second case study (Table 1).
3) C type bora episode No. 82 was selected as the third case study (Table 1, Lepri et al.).
4) C type bora episode No. 10 was selected as the fourth case study (Table 1).
5) U type bora episode No. 63 was selected as the fifth case study (Table 1, Lepri et al.).
6) U type bora episode No. 40 was selected as the sixth case study (Table 1).

Bora episodes in the first and the second case study are separated by a gap in wind speed and direction data, removed during preprocessing stage.
Similar to first two case studies, at 60 m height during the sixth case study there is removed data. Here, bora episodes are not separated due to consistent data at 80 m height.

4.2.1 First case study

Bora episodes 80 and 81 lasted from March 6 to 9, 2011. First episode lasted from March 6 to 8 and the second one lasted for one day. For 10 m and for 40 m height (Figure 13), observed wind speed increased during March 6 and reached its first maximum value of approximately 20 ms^{-1} in the night of March 7, for which MSLP map is shown in Figure 12a.

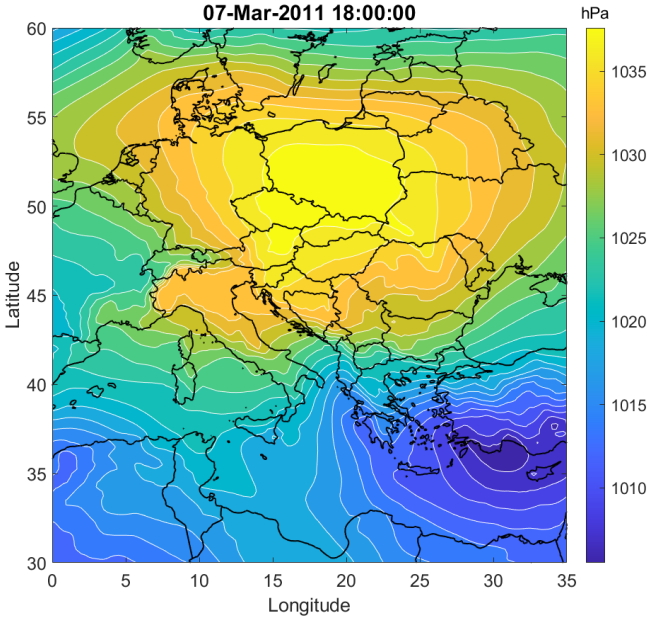

(a) *MSLP map on March 7, 2011, at 18:00.*

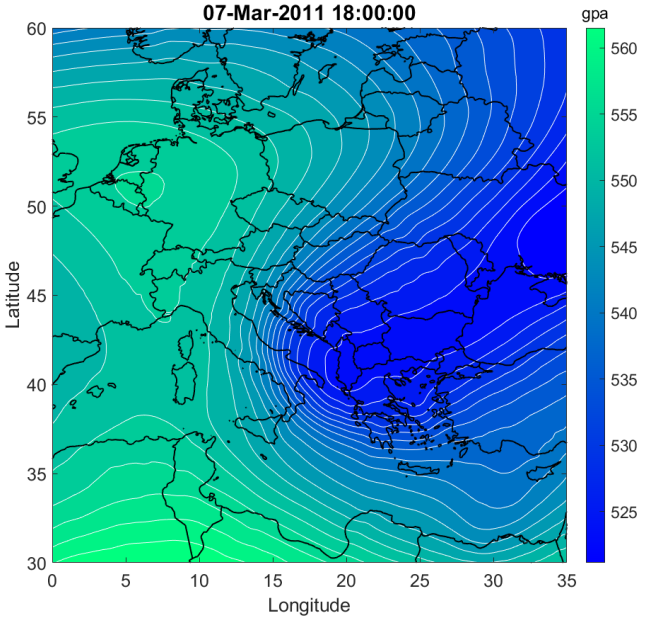

(b) *500-hPa geopotential height on March 7, 2011, at 18:00.*

Figure 12: *Synoptic setting during bora episode No. 80 (Table 1 from Lepri et al.). Both subfigures are reproduced from ERA5 data. This is the case for all subsequent figures.*

Thorough in geopotential height that stretched from the northeastern Europe towards the western Balkans was present at the same time (Figure 12b). Both CERRA and WRF reproduce the starting and ending time of bora episodes, as well as the general shape of wind speed time series, with high accuracy. Observed peak wind values on March 7 are not reproduced by CERRA or WRF. Overall wind speed value is better represented with WRF than with CERRA.

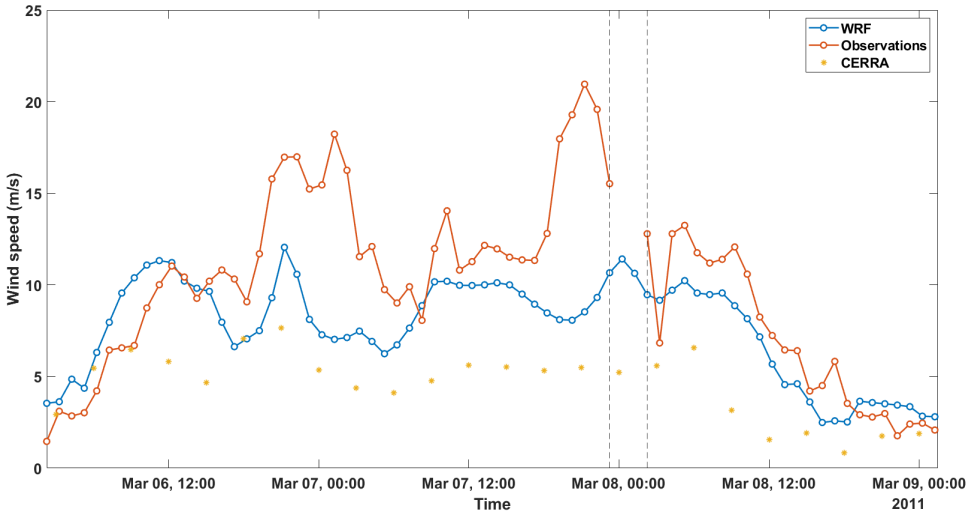

(a) *Hourly-averaged wind speed values at 10m.*

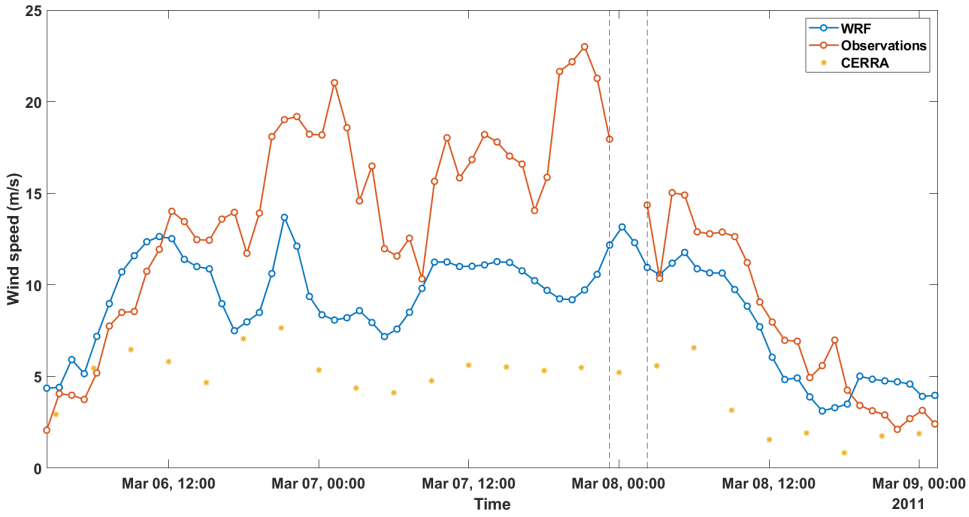

(b) *Hourly-averaged wind speed values at 40m.*

Figure 13: *Time series of CERRA, WRF and observed wind speed for bora episodes No. 80 and 81. Vertical dashed lines separate the two bora episode (4.2).*

4.2.2 Second case study

In 2018, bora episode No. 35 lasted from mid-day of 24 to morning of 26 September. Bora episode No. 36 followed immediately after and lasted for a day and a half. High and low pressure centers displayed on September 26 (Figure 14a), as well as a thorough in geopotential height at 500 hPa (Figure 14b), are similar to the ones displayed in Figure 14.

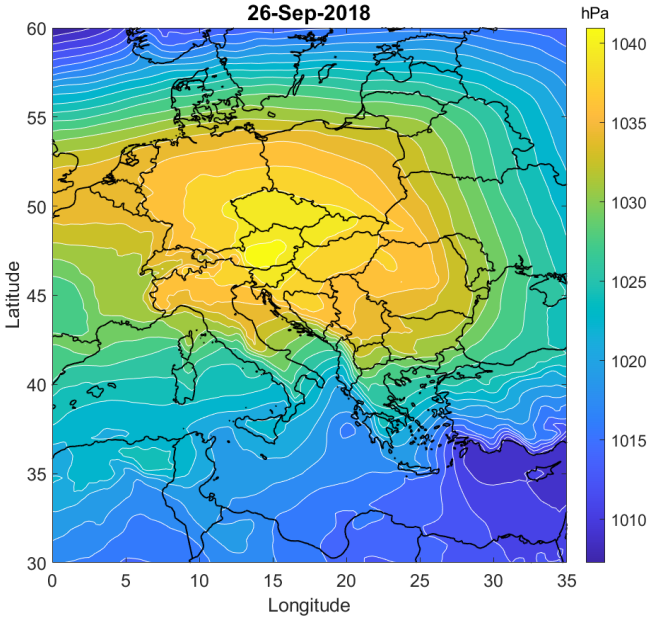

(a) *MSLP on September 26, 2018, at midnight.*

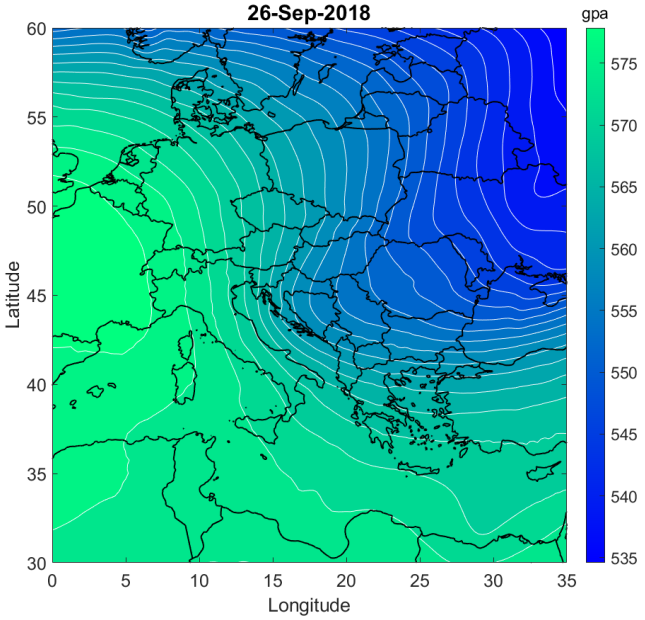

(b) *500-hPa geopotential height on September 26, 2018, at midnight.*

Figure 14: *Synoptic setting during bora episode No. 35. (Table 1).*

CERRA underestimates average wind speed in the first bora episode by 7.7 $ms^{-}1$ at 60 m and by 6.7 $ms^{-}1$ at 80 m height. WRF reduces this to 6.6 $ms^{-}1$ and 5.3 $ms^{-}1$, respectively. Wind speed maximum of approximately 25 $ms^{-}1$ was observed during afternoon of September 24 and is not reproduced by WRF or CERRA (Figures 15). During the following A type bora episode, CERRA and WRF wind speed is in alignment with measurements, following the observed oscillation of wind speed in between evening and morning hours.

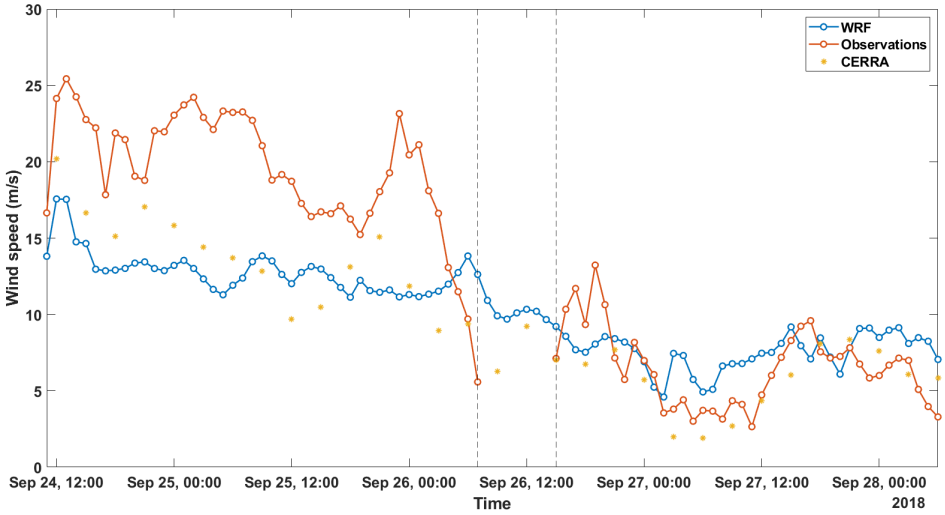

(a) *Hourly-averaged wind speed values at 60m.*

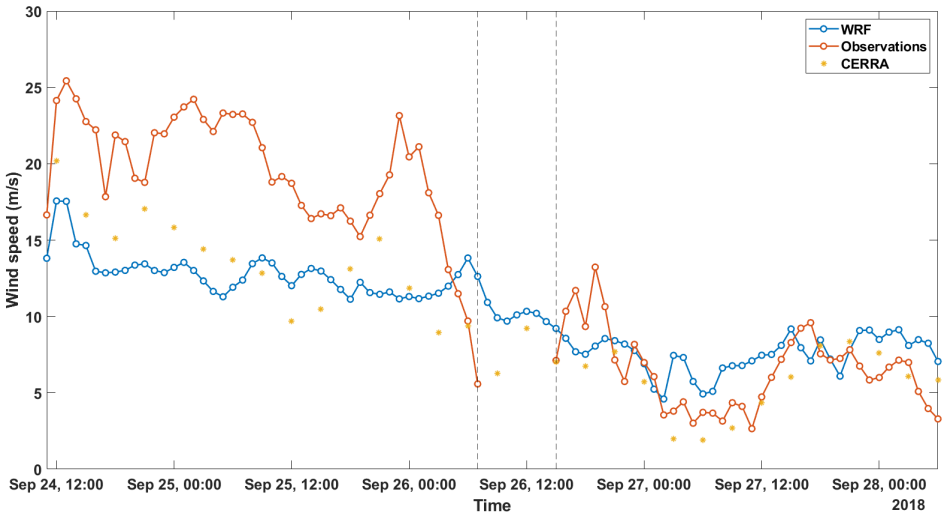

(b) *Hourly-averaged wind speed values at 80m.*

Figure 15: *Time series of CERRA, WRF and observed wind speed for bora episode 35 and 36. Vertical dashed lines separate the two bora episode (4.2).*

4.2.3 Third study case

In the afternoon of March 20 2011, during bora episode No. 82 (Table 1 [3]), a regional pressure low was placed over central and eastern Mediterranean (Figure 16a). It was accompanied by a thorough in geopotential heigh distribution, stretching from northeastern Europe towards central Mediterranean, with a regional low found over south Italy (Figure 16b).

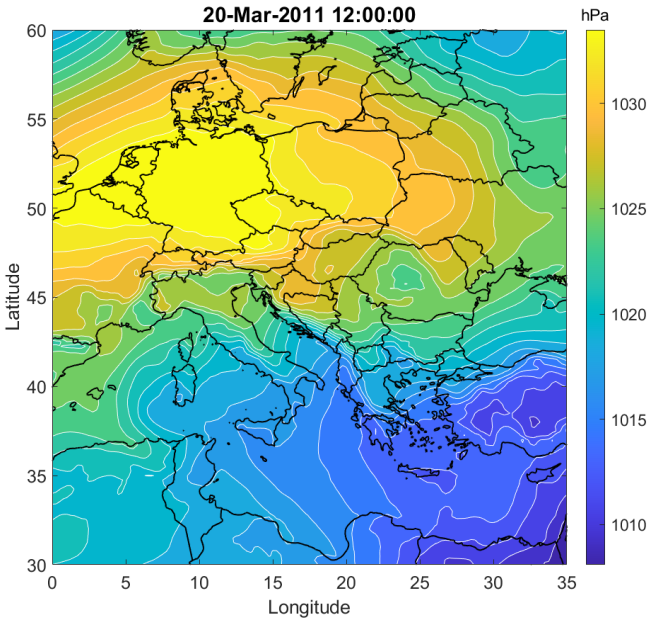

(a) *MSLP on March 20 at 12:00, 2011.*

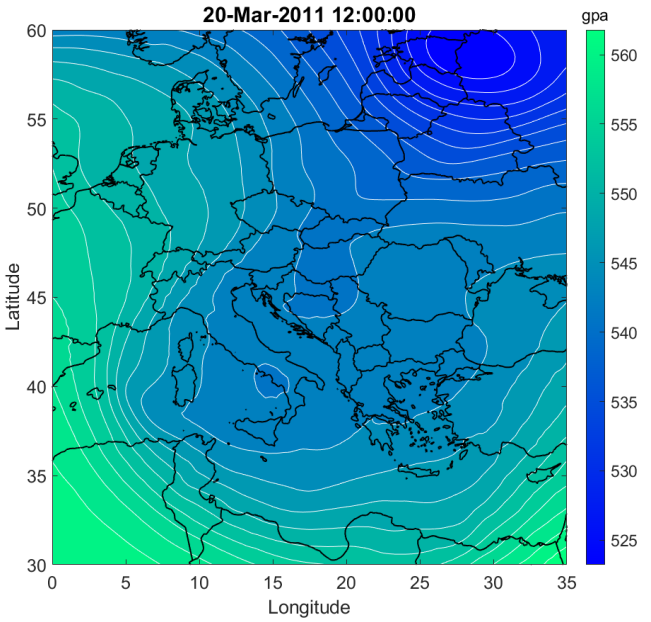

(b) *500-hPa geopotential height on March 20 at 12:00, 2011.*

Figure 16: *Synoptic setting during bora episode No. 82 (Table 1 from Lepri et al.).*

Measured wind speed increased slowly to its maximum value of approximately 18 $ms^{-}1$ in the evening of 20th March at both 10 m (Figure 17a) and 40 m (Figure 17b) heights. WRF reproduced wind speed follows the trend of the observed values at 10 and 40m level. CERRA repetitively underestimates observed wind speed during the afternoon of each day for which it displays a daily minimum, not shown by the measurements. Largest underestimation of wind speed value by CERRA and WRF is noticed during the observed wind speed maximum at around midnight, March 21, reaching the difference of more than 7 $ms^{-}1$ at both heights (Figure 17).

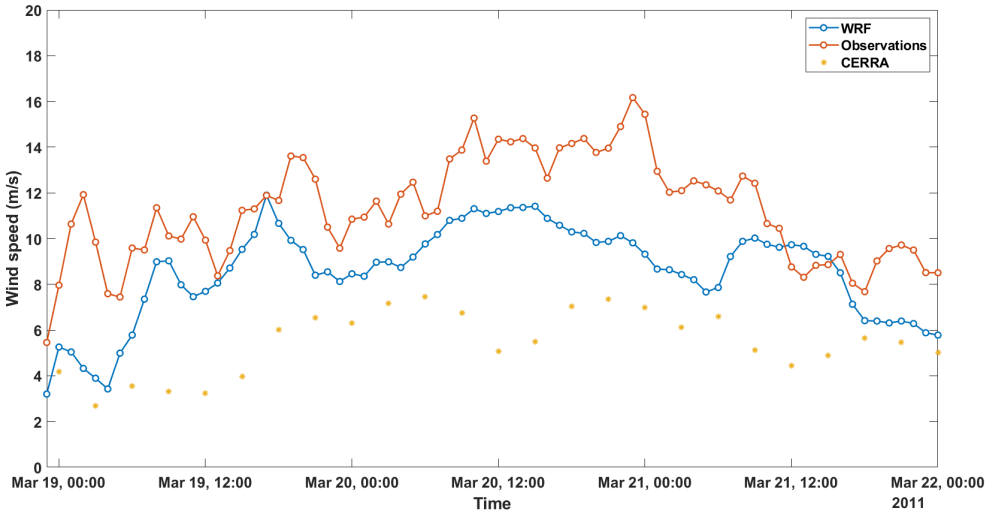

(a) *Hourly-averaged wind speed values at 10m.*

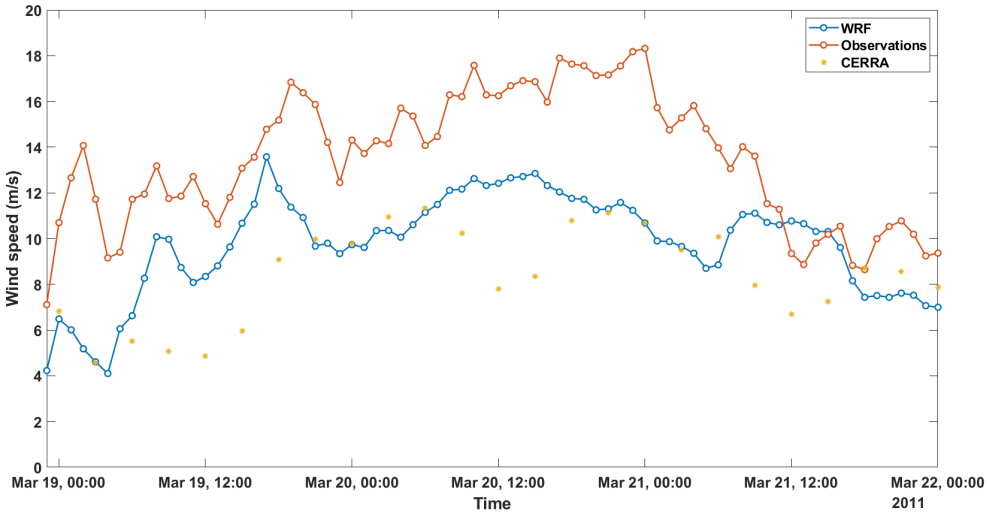

(b) *Hourly-averaged wind speed values at 40m.*

Figure 17: *Time series of CERRA, WRF and observed wind speed for bora episode No. 82.*

4.2.4 Fourth case study

Bora event number 10 (Table 1), lasting from March 20 to 24, 2018, occurred when a pressure low was located over central Mediterranean and pressure high over western Europe (Figure 18a). Geopotential height map for this Bora event (Figure 18b) has the same features as the one shown in Figure 16b.

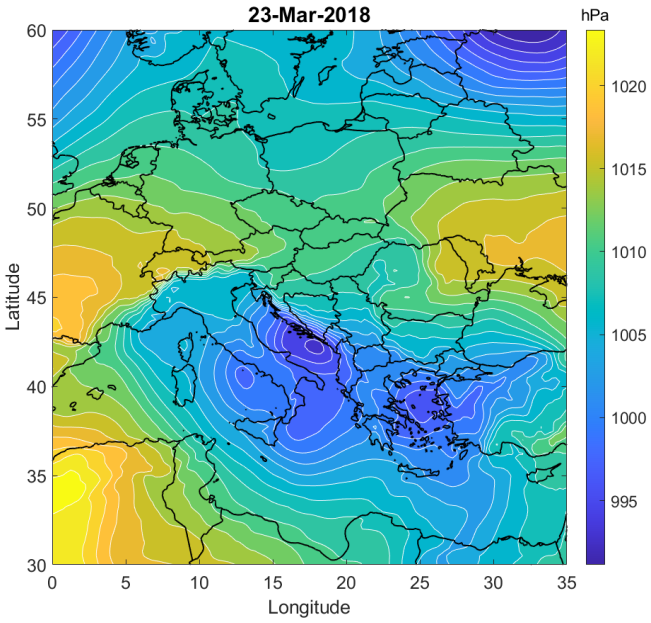

(a) *MSLP on March 23 at midnight, 2018..*

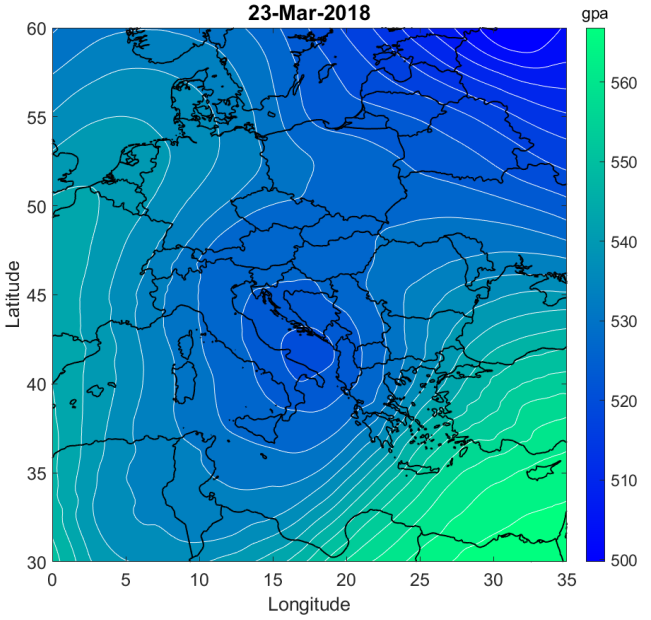

(b) *500-hPa geopotential height on March 23 at midnight, 2018.*

Figure 18: *Synoptic setting during bora episode No. 10 (Table 2).*

In the evening of March 20 observed bora wind speed increased sharply to values of around 16 $ms^{-}1$. Same behavior is reproduced by both CERRA and WRF. Considerable wind speed underestimation is noticed when compared to measured data, up to 8 ms^{-1} during nights of March 22-24 at 60 m (Figure 19a) and up to 6 ms^{-1} at 80 m (Figure 19b) height. Wind speed values during the bora episode are better reproduced with WRF.

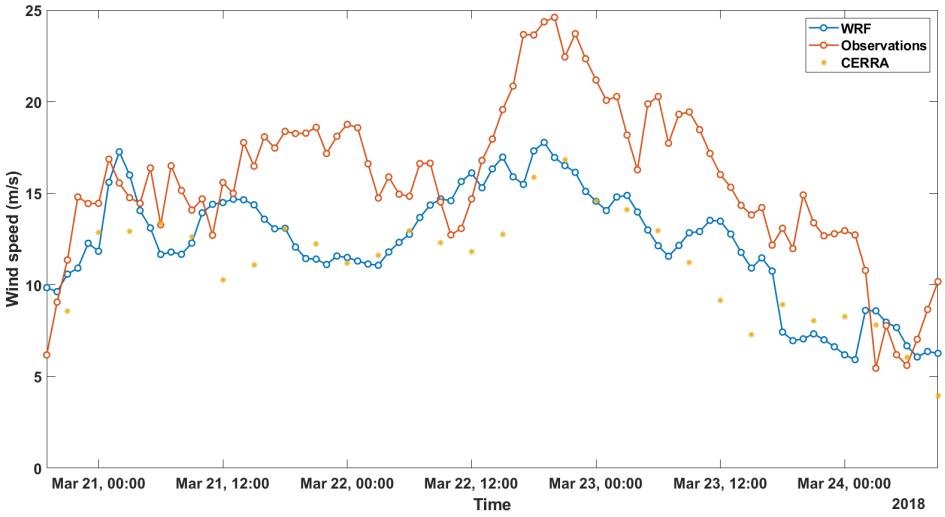

(a) *Hourly-averaged wind speed values at 60m.*

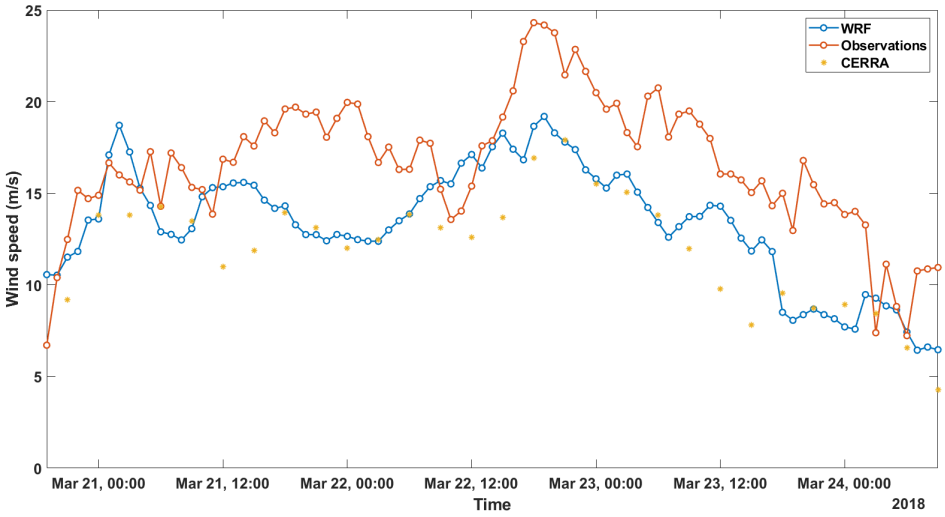

(b) *Hourly-averaged wind speed values at 80m.*

Figure 19: *Time series of CERRA, WRF and observed wind speed for bora episode No. 10.*

4.2.5 Fifth case study

Period from January 20 to 24 2011 is marked as bora episode No. 63 (Table 2 [3]). It displayed a pressure low over central Mediterranean on January 21 at midnight (Figure 20a), that slowly moved southeast in the period of five days and reached eastern Mediterranean around January 24 (Figure 21a).

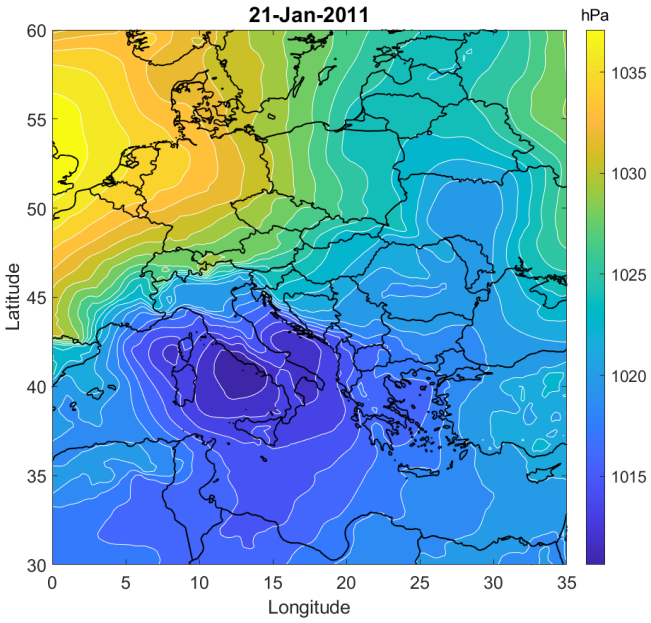

(a) *MSLP on January 21 at midnight, 2011.*

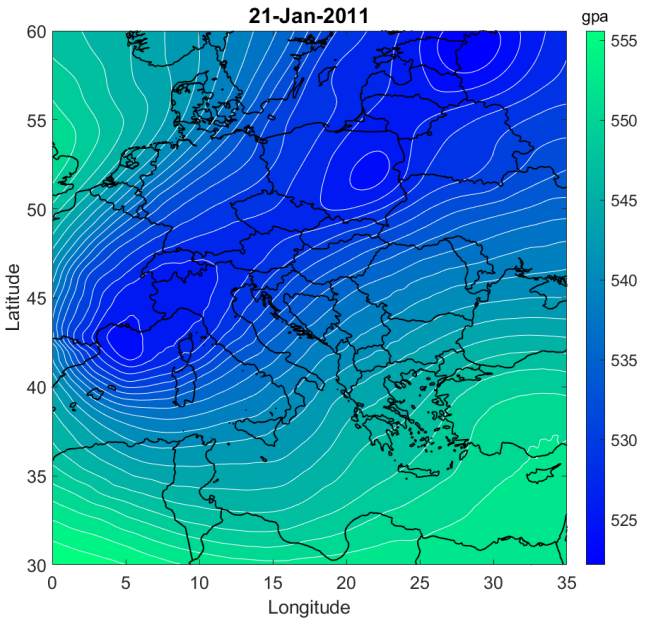

(b) *500-hPa geopotential height on January 21 at midnight, 2011.*

Figure 20: *Synoptic setting at the beginning of bora episode No. 63 (Table 1 from Lepri et al.)*

Thorough in geopotential heigh stretched from northeastern Europe and reached bay of Genoa in the beginning of Bora episode (Figure 20b). Its extent was shortened by January 24 and reached the western Balkans (Figure 21b).

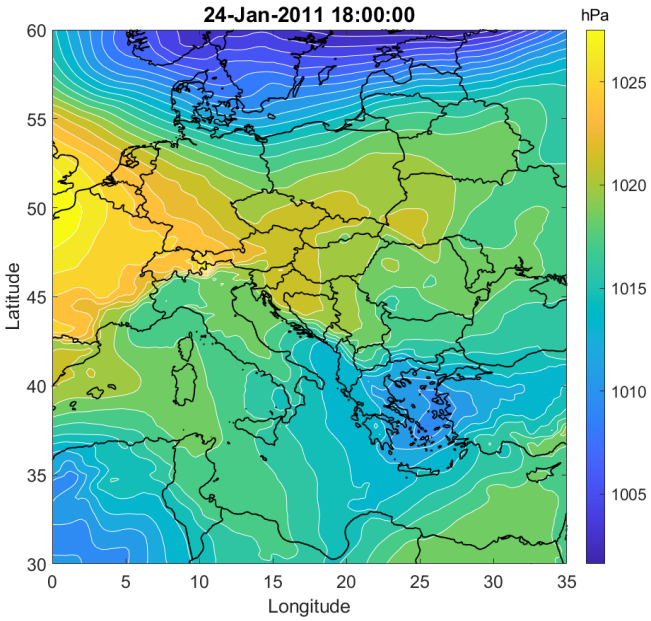

(a) *MSLP on January 24 at 18:00, 2011.*

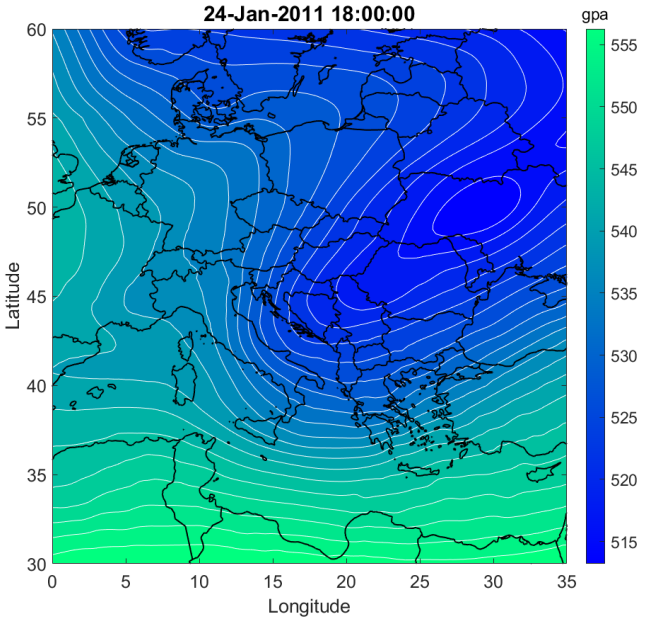

(b) *500-hPa geopotential height on January 24st at 18:00, 2011.*

Figure 21: *Synoptic setting at the ending of bora episode number 63.*

From the evening of January 20 until morning of 23, wind speeds were high, reaching maximum value over 20 ms^{-1} in the evening of January 22 at 10 (Figure 22a) and 40 m (Figure 22b). At 10 m height, CERRA underestimated measured winds by 15 ms^{-1}, while WRF preformed slightly better, underestimating the observed winds by 10 ms^{-1}. On 40m level, underestimation of observed wind speed does not extend over 8 ms^{-1} for both WRF and CERRA. In the night of January 24, CERRA overestimates observed wind speed values by 2 to 3 $ms^{-}1$ at 40m level. At the end of Bora event, an increase in wind speed is again observed, and it is reproduced by WRF and CERRA to a lesser extent.

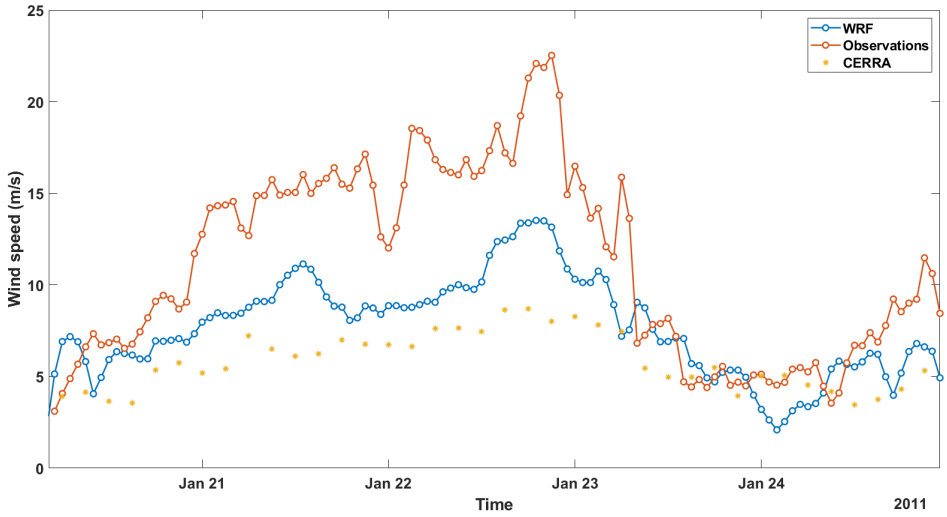

(a) *Hourly-averaged wind speed values at 10m.*

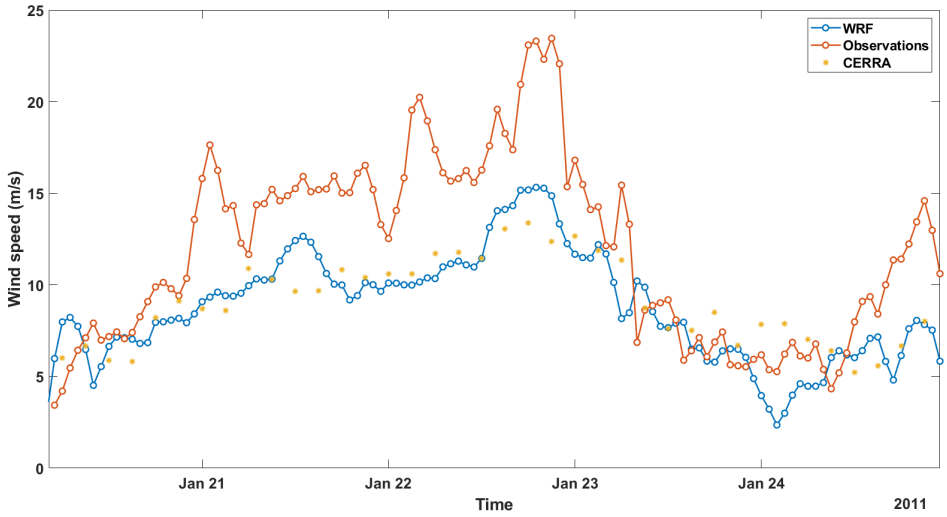

(b) *Hourly-averaged wind speed values at 40m.*

Figure 22: *Time series of CERRA, WRF and observed wind speed for bora episode No. 63.*

4.2.6 Sixth case study

During the bora episode No. 40 (Table 1) that started on November 27 and lasted until November 30 2018, central Mediterranean pressure low was recorded on the evening of November 27 (Figure 23a). It was replaced by a pressure high centered over the eastern Europe with a regional low over eastern Mediterranean in the evening of November 29 (Figure 24a).

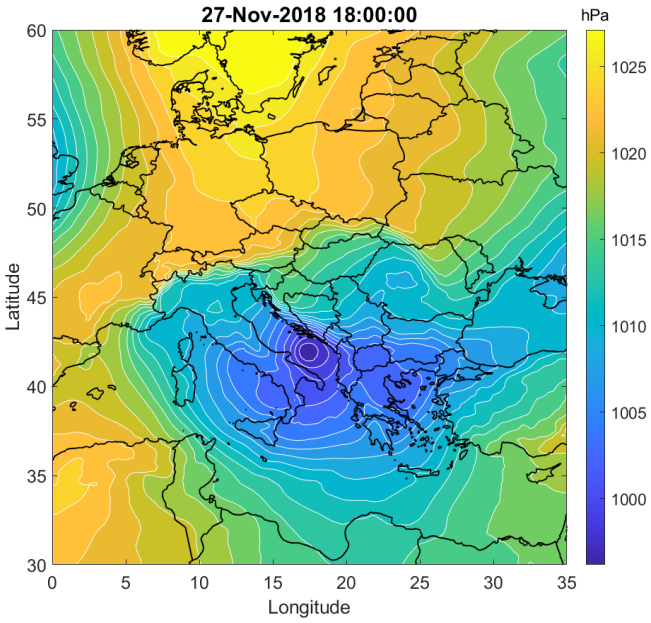

(a) *MSLP on November 27 at 18:00, 2018.*

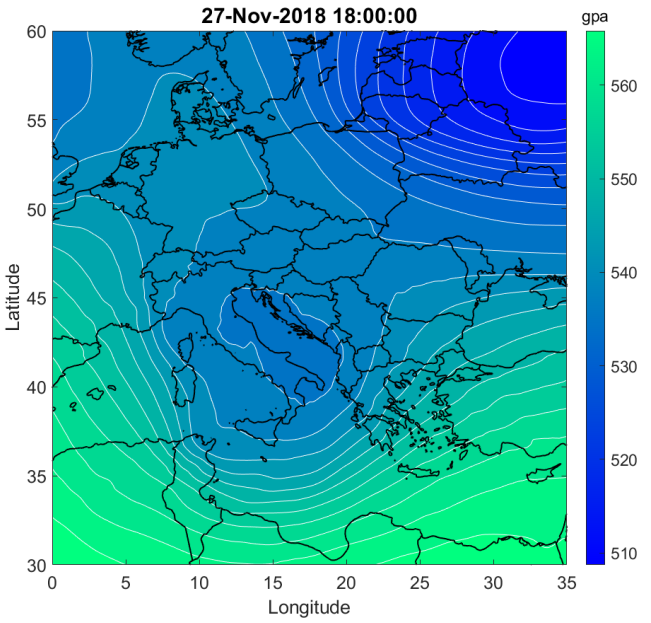

(b) *500-hPa Geopotential height on November 27 at 18:00, 2018.*

Figure 23: *Synoptic setting at the beginning of Bora episode No. 40 (Table 1).*

Evolution of geopotential height during the bora episode is shown in Figures (23b) and (24b). It shows a regional low of geopotential height over central Mediterranean on November 27 that was displaced eastwards on November 29.

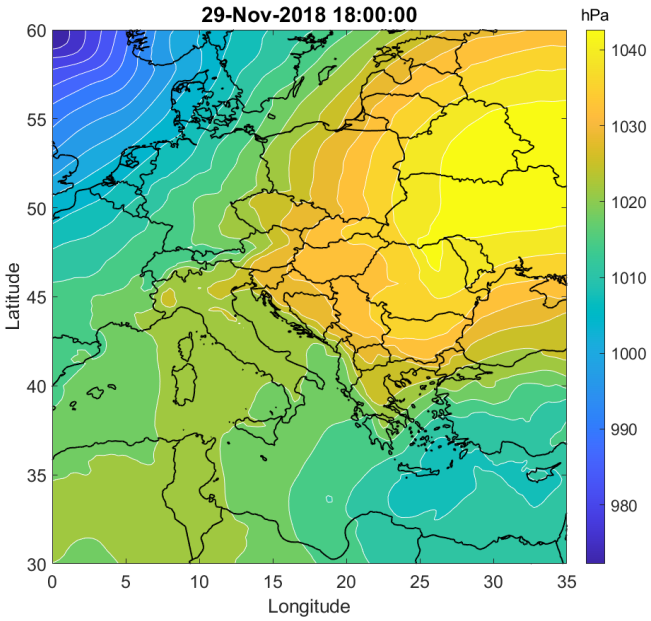

(a) *MSLP map on November 29 at 18:00, 2018.*

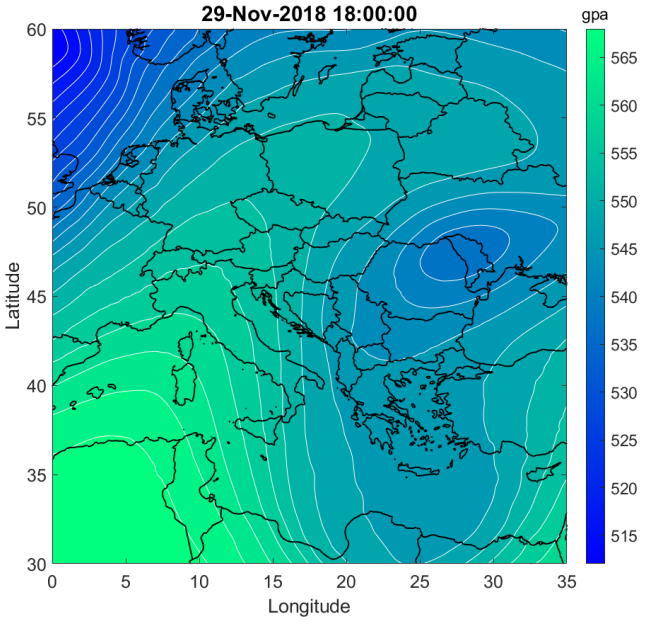

(b) *Geopotential height at 500hPa on November 29 at 18:00, 2018.*

Figure 24: *Synoptic map of Europe during the ending of bora episode number 40.*

Observed wind speed during the first two days of Bora event reaches values of 21 $ms^{-}1$ at 60 m and is high when compared to wind speed measured from November 29 until the end of bora episode (Figure 25b). At 80 m height, observed maxima of wind speed do not exceed 19 ms^{-1}. Beginning and ending of bora episode are well represented by both WRF and CERRA. Observed wind speed from November 29 until the end of the bora episode ranges from 2 to 10 ms^{-1} and is overestimated up to 7 ms^{-1} by the WRF model, and by up to 5 ms^{-1} by the CERRA model.

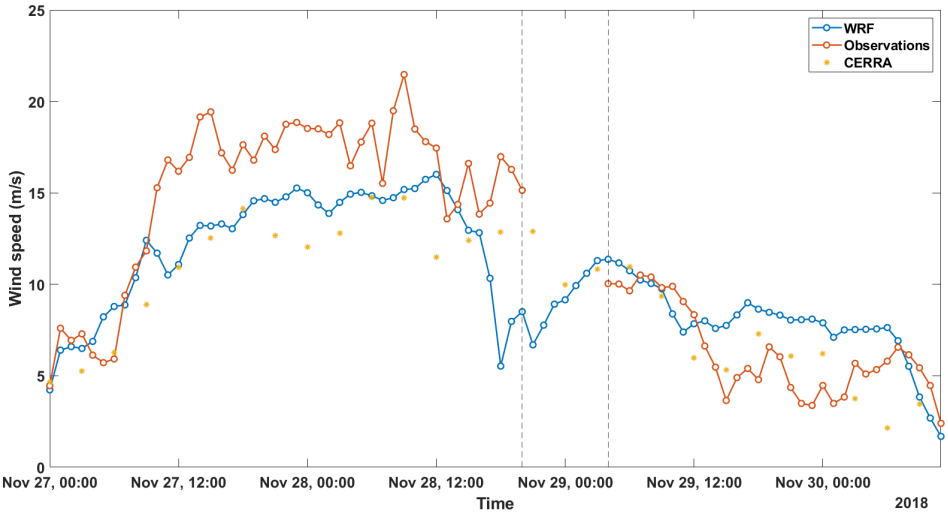

(a) *Hourly-averaged wind speed values at 60m. Vertical dashed lines denote the zone with filtered out values (4.2).*

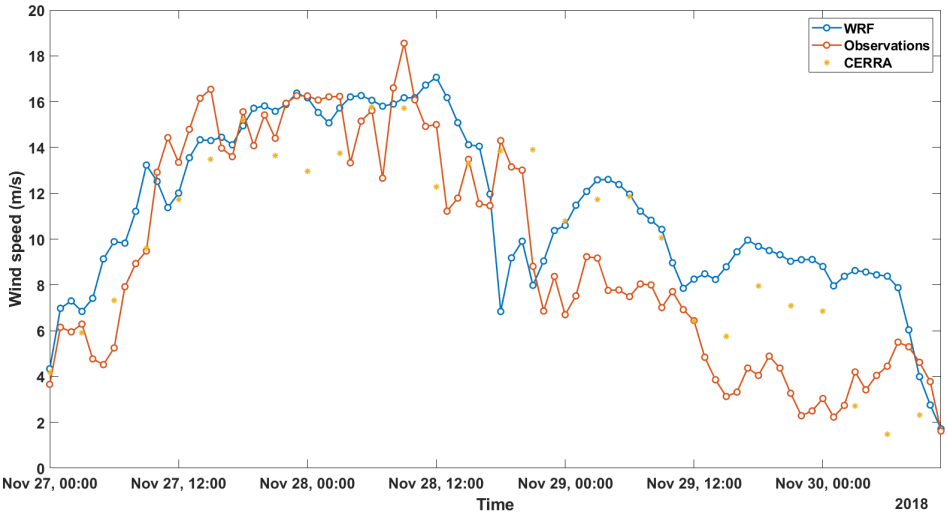

(b) *Hourly-averaged wind speed values at 80m.*

Figure 25: *Time series of CERRA, WRF and observed wind speed for bora episode No. 40.*

5 Discussion and Conclusion

During most of bora episodes in 2018, it is shown that measuring anemometer at 60m hub height has slightly higher wind speed values than the one placed at 80m hub height. This could be due to downslope acceleration of Bora wind [1]. 80m wind turbine is placed at the peak height of Pometeno Brdo, while 60m wind turbine is located approximately 250 m in southwestern direction at 14 m lower mean sea level height (Figure 2).

JC-WT scheme categorization enabled focusing on distinct Bora synoptical types, recognizing anticyclonic and cyclonic weather patterns over Croatia with sufficient accuracy for selected case studies. Periods longer than three days were mostly categorized as U type, because of the dynamical changes of synoptical setting over a few days. "A type" bora episodes were found accompanied by a strong directional bora type event preceding them (e.g. 4.2.2). This behavior could be prescribed to an anticyclonic bora development, where high MSLP field over central Europe expands toward Balkan peninsula [13]. Also, "C type" bora episodes were found after or before strong directional type bora episodes (not shown). This behavior could be correlated to cyclonic bora, during which MSLP low over central Mediterranean transitions towards Adriatic Sea and is further displaced in the southeastern direction [13].
Weather index histograms (Figure 11) also show that in the upper 60 and 80m levels most of the bora episodes display intense directional E and NE type with A and C type being much rarer than in bora episodes recorded at 10 to 40m levels. This could be due to relatively short duration of "A type" and "C type" bora episodes which are not separated as a standalone episode in 2018. Hourly averaged wind direction data provided by Končar d.o.o. could be the reason for this, as information on sub-hourly changes of wind direction is missing.
Although JC-WT method proves to be insightful, synoptic categorization such as one performed by Šoljan et al. [14] is recommended for better understanding of bora characteristics.

The 10m level wind speed is severely underestimated in CERRA reanalysis for bora episodes, as seen in section 4.1. Although, statistical analysis of 10 m wind reproduced by CERRA have shown satisfactory results over regions with similar orography, e.g. Greece [6], unclear generating mechanisms of bora in Dalmatia [10] and a coarse 5.5 km CERRA spatial resolution prove to be a significant obstacle in its representation at near-ground level. These shortcomings are also visible at upper layers of atmosphere where CERRA significantly underestimates the wind speed during high intensity bora periods of more than 10 ms^{-1} (8) and (10).

WRF downscaling to 1km improves the wind speed reproduction with average underestimation of observed wind speed per case ranging from 1.8 $ms^{-}1$ to 3.8 $ms^{-}1$ (3) at different heights. Orographic features such as mountain passages and steep mountain slopes are better represented with higher resolution and have a direct connection to reproductive quality of bora flow intensity [10]. Although WRF improves overall wind speed average during a bora episode, significant biases of up to 10 ms^{-1} are noted in each case study during strong wind periods. Similar biases are obtained for the complex terrain of the northern Iberian mountain range [15]. At heights above 40m (25b), both WRF and CERRA show occasional overestimation of bora wind speed during the milder bora periods. This overestimation of wind speed produced by CERRA is also detected in the Northern Sea, at heights of 100 m [5].

It can be concluded that CERRA reanalysis reproduces main bora features at Pometeno Brdo well in different synoptic settings with underwhelming results at reproducing strong hourly periods of bora wind. The WRF model with 1 km resolution reproduces wind better, especially near-ground, but still falls short when representing stronger wind episodes. Also, CERRA presents a valuable dataset for analysis of bora characteristics at wind turbine heights.
Increase in input terrain resolution for WRF could improve the results of the simulation and closer systematic inspection of all categorized bora episodes could provide more insight bora behavior different heights. Further analysis could be done to compare the results of the WRF and CERRA to similar, high wind potential locations in Dalmatia to get more knowledge on spatial and temporal distribution of bora flow in this region. Additionally, research on micro- and mesoscale bora characteristics and advancements in computing resources are crucial for better understanding of bora in Dalmatia.

6 Bibliography

[1] Branko Grisogono, Danijel Belušić: *A review of recent advances in understanding the meso- and microscale properties of the severe Bora wind*, Tellus A, Volume61, Issue1, January 2009, Pages 1-16
URL: https://doi.org/10.1111/j.1600-0870.2008.00369.x

[2] Vesna Jurčec, Smiljan Visković: *Mesoscale characteristics of southern Adriatic bora storms*, Geofizika, Vol. 11 No. 1, 33-46, 1994..
URL: https://hrcak.srce.hr/20021

[3] Lepri et al.:*Bora wind characteristics for engineering applications*, Wind and Structures, Vol. 24, No. 6 (2017) 579-611.
URL: https://doi.org/10.12989/was.2017.24.6.579

[4] Horvath, Kristian, Kosović, Branko: *Multiscale simulations of bora downslope windstorm events*, 35th International Conference on Alpine Meteorology, Riva del Garda, Italija, 02.09.2019-06.09.2019

[5] Spangehl, Thomas and Borsche, Michael and Niermann, Deborah and Kaspar, Frank and Schimanke, Semjon and Brienen, Susanne and Möller, Thomas and Brast, Maren: *Intercomparing the quality of recent reanalyses for offshore wind farm planning in Germany's exclusive economic zone of the North Sea*, Advances in Science and Research, Vol. 20,(2023) 109-128.
URL: https://doi.org/10.5194/asr-20-109-2023

[6] Galanaki, E. et al.: *Validating the Copernicus European Regional Reanalysis (CERRA) Dataset for Human-Biometeorological Applications.*, Environ. Sci. Proc. 2023, 26, 111.
URL: https://doi.org/10.3390/environsciproc2023026111

[7] Kine Solbakken and Yngve Birkelund: *Evaluation of the Weather Research and Forecasting (WRF) model with respect to wind in complex terrain*, Journal of Physics: Conference Series, Volume 1102, WindEurope conference 2018 within the Global Wind Summit 25–28 September 2018, Hamburg, Germany
DOI: 0.1088/1742-6596/1102/1/012011

[8] BELUŠIĆ, D. and KLAIĆ, Z.B.: *Estimation of bora wind gusts using a limited area model.* ,Tellus A, 56: 296-307, 2004.
URL: https://doi.org/10.1111/j.1600-0870.2004.00068.x

[9] Janić, Zaviša I.: *Nonsingular implementation of the Mellor-Yamada level 2.5 scheme in the NCEP Meso model*,Office note (National Centers for Environmental Prediction (U.S.)) ; 437, 2001.
URL: https://repository.library.noaa.gov/view/noaa/11409

[10] Milivoj Kuzmić et al.:*TerraSAR-X observations of the northeastern Adriatic bora: Early results*, Acta Adriatica, Vol. 54 No. 1, 13-26., 2013.
URL: https://hrcak.srce.hr/115706

[11] Dražken Poje: *Wind persistence in Croatia*, The International Journal of Climatology, Volume12, Issue6 ,September/October 1992, Pages 569-586.
URL: https://doi.org/10.1002/joc.33701206041

[12] Jenkinson A, Collison F: *An initial climatology of gales over the north sea.*, Synoptic climatology branch memorandum. Meteorol Off 62, 1977

[13] Vesna Jurčec: *SEVERE ADRIATIC BORA STORMS IN RELATION TO SYNOPTIC DEVELOPMENTS*, Hrvatski meteorološki časopis, 24 (24), 11-20, 1989
URL: https://hrcak.srce.hr/69265

[14] Šoljan, V.; Belušić, A.; Šarović, K.; Nimac, I.; Brzaj, S.; Suhin, J.; Belavić, M.; Večenaj, Ž.; Grisogono, B.: *Micro-Scale Properties of Different Bora Types.* , Atmosphere 2018, 9, 116.
URL: https://doi.org/10.3390/atmos9040116

[15] Sergio Fernández-González et al.: *Sensitivity Analysis of the WRF Model: Wind-Resource Assessment for Complex Terrain*, Journal of Applied Meteorology and Climatology, Volume 57, Issue 3, 733–753, 2018.
URL: https://doi.org/10.1175/JAMC-D-17-0121.1

A The Jenkinson-Collison automated Lamb Weather Typing Classification scheme

A 16 point grid is centered over the case study (Figure 26). Based on the mean sea level pressure for this 16 point grid, the southerly, westerly and total component of the geostrophic surface flow and shear velocity are calculated.

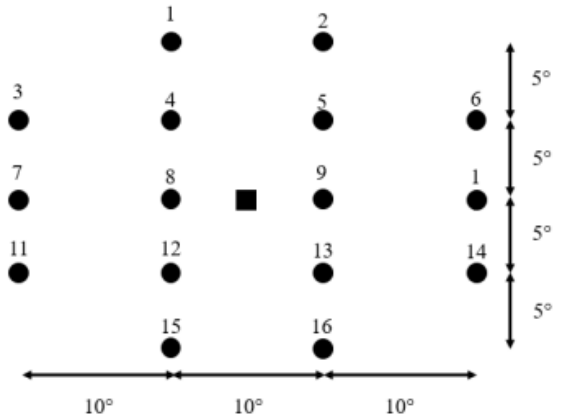

Figure 26
Spacing and numbering in the 16 point grid system for the Jenkinson-Collision automated Lamb weather typing classification scheme.

Assuming p_i is the pressure in point i of the 16 point grid, Ψ the latitude of the case study/grid center (black sqaure in Figure 26), then the southerly flow (SF), westerly flow (WF), total flow (F), southerly shear vorticity (ZS), westerly shear vorticity (ZW) and total shear vorticity (Z) are calculated following equations (A.1):

$$WF = 0.5(p_{12} + p_{13}) - 0.5(p_4 + p_5)$$

$$SF = \frac{1}{cos(\Psi)}[0.25(p_5 + 2p_9 + p_{13}) - 0.25(p_4 + 2p_8 + p_{12})]$$

$$F = (SF^2 + WF^2)^{\frac{1}{2}}$$

$$ZS = \frac{sin(\Psi)}{sin(\Psi - 5)}[0.25(p_6{+}2p_{10}{+}p_{14}){-}0.25(p_5{+}2p_9{+}p_{13}){-}0.25(p_4{+}2p_8{+}p_{12}){+}0.25(p_3{+}2p_7{+}p_{11})]$$

$$ZW = \frac{sin(\Psi)}{sin(\Psi + 5)}[0.5(p_{15} + p_{16}) - 0.5(p_8 + p_9)]^{-\frac{1}{2}}(cos(\Psi))^2[0.5(p_8 + p_9) - 0.5(p_1 + p_2)]$$

$$Z = ZS + ZW \tag{A.1}$$

The flow direction is calculated using Eq. (S2) and 45° sector is assigned for a 8 direction compass. If the outcome of eauation (A.2) is positive, 180° is added.

$$direction = \frac{1}{tan(\frac{WF}{SF})} \tag{A.2}$$

Based on an inter-comparison of the flow indices (SF, WF, F, ZS, ZW and Z) and the flow direction, 27 different weather types (WTs) are identified. The inter-comparison of the flow indices considers following criteria:

$|Z| < F$: pure directional WT (including 8 WTs according to the flow direction)

$|Z| > 2F$ and $Z > 0$: pure cyclonic WT

$|Z| > 2F$ and $Z < 0$: pure anti-cyclonic WT

$F < |Z| < 2F$ and $Z > 0$: hybrid cyclonic WT (including 8 WTs according to the flowdirection)

$F < |Z| < 2F$ and $Z < 0$: hybrid anti-cyclonic WT (including 8 WTs according to the flow direction)

$F < 6$ and $Z < 6$: undefined WT